ARTICLE IN PRESS

Nature Communications

https://doi.org/10.1038/s41467-026-71132-5

Article in Press

Expanding the targeted protein degradation approach with small molecule chimeras directed to the 26S proteasome

Received: 2 July 2024

Accepted: 16 March 2026

Cite this article as: Casasampere, M., Carneros, H., Roda, T. *et al.* Expanding the targeted protein degradation approach with small molecule chimeras directed to the 26S proteasome. *Nat Commun* (2026). https://doi.org/10.1038/s41467-026-71132-5

Mireia Casasampere, Hector Carneros, Tania Roda, Alice Zuin, Núria Gallisà-Suñé, Alba González-Artero, Bernat Coll-Martínez, José Luis Abad, Abdulateef Alqahtani, Josefina Casas, Patricia Fernández-Nogueira, Antonio Delgado, Jordi Bujons, Gemma Fabriàs & Bernat Crosas

We are providing an unedited version of this manuscript to give early access to its findings. Before final publication, the manuscript will undergo further editing. Please note there may be errors present which affect the content, and all legal disclaimers apply.

If this paper is publishing under a Transparent Peer Review model then Peer Review reports will publish with the final article.

ARTICLE IN PRESS

© The Author(s) 2026. **Open Access** This article is licensed under a Creative Commons Attribution-NonCommercial-NoDerivatives 4.0 International License, which permits any non-commercial use, sharing, distribution and reproduction in any medium or format, as long as you give appropriate credit to the original author(s) and the source, provide a link to the Creative Commons licence, and indicate if you modified the licensed material. You do not have permission under this licence to share adapted material derived from this article or parts of it. The images or other third party material in this article are included in the article's Creative Commons licence, unless indicated otherwise in a credit line to the material. If material is not included in the article's Creative Commons licence and your intended use is not permitted by statutory regulation or exceeds the permitted use, you will need to obtain permission directly from the copyright holder. To view a copy of this licence, visit http://creativecommons.org/licenses/by-nc-nd/4.0/.

ARTICLE IN PRESS

Expanding the targeted protein degradation approach with small molecule chimeras directed to the 26S proteasome

Mireia Casasampere[1+], Hector Carneros[1+], Tania Roda[1+], Alice Zuin[2+], Núria Gallisà-Suñé[2], Alba González-Artero[2], Bernat Coll-Martínez[2], José Luis Abad[1], Abdulateef Alqahtani[1], Josefina Casas[1,3], Patricia Fernández-Nogueira[4], Antonio Delgado[1,5], Jordi Bujons[1*], Gemma Fabriàs[1,3*] & Bernat Crosas[2*]

1 Department of Biological Chemistry
Institute for Advanced Chemistry of Catalonia (IQAC-CSIC)
Jordi Girona 18, 08034-Barcelona, Spain

2 Department of Structural and Molecular Biology
Molecular Biology Institute of Barcelona (IBMB-CSIC)
Baldiri Reixac 4, 08028-Barcelona, Spain

3 CIBER of Hepatic and Digestive Diseases (CIBEREHD)
Instituto de Salud Carlos III (ISCIII)
Carretera de Majadahonda - Pozuelo, Km. 2.200. 28220 - Majadahonda (Madrid), Spain

4 Department of Biomedicine
School of Medicine and Health Sciences, University of Barcelona
Casanova, 143, 08036 Barcelona, Spain

5 Department of Pharmacology, Toxicology and Medicinal Chemistry
Faculty of Pharmacy and Food Sciences, University of Barcelona
Av. de Joan XXIII, 27-31, 08028 Barcelona, Spain

+ These authors contributed equally to this work.

* Correspondence to: jordi.bujons@iqac.csic.es, gemma.fabrias@iqac.csic.es, or bernat.crosas@ibmb.csic.es

ARTICLE IN PRESS

Abstract

Classical proteolysis targeting chimeras (Protacs) bind specific targets and E3 ubiquitin-ligases, promoting ubiquitination and degradation of targets by the proteasome. Multiple chimeras that degrade proteins relevant in several diseases have been developed, and the number is quickly increasing, indicating their therapeutic projection. Given the specificities of proteolytic pathways and limitations in E3-based Protacs, alternative strategies in targeted protein degradation are pursued. Herein, using two targets relevant in oncology as models (IMPDH2 and CERT1), we provide proof of concept for 26S-oriented compounds based on small-molecule ligands of USP14, a 26S-associated deubiquitinase involved in substrate processing and allosteric regulation of 26S activity. Our findings will expand the potential of targeted protein degradation.

Introduction

Targeted protein degradation (TPD) is a powerful strategy of inactivation of key players in human diseases, offering mechanistic advantages as compared to classical inhibition[1,2]. The development of proteolysis targeting chimeras (Protacs) has generated multiple compounds with drug profile[1–3], with some currently in clinical trials[4]Despite the rise in Protacs progress, several aspects, such as the reduced number of small molecule ligands adaptable for chimera building and the generally poor Protacs

ARTICLE IN PRESS

solubility[5–7] limit E3-based Protacs implementation. Proper levels and activation state of the ligase (in target tissues), productive engagement of the substrate, and accessibility of the ligase to lysine residues on the target represent additional intrinsic limitations that curtail the effectiveness of some E3-based Protacs[5–8].The 26S proteasome is conformed of the core particle (20S or CP), a cylindrical proteolytic complex, and the regulatory particle (19S or RP), consisting of the lid and base subcomplexes (Fig. 1a)[9–12] In the base, the hexameric ring of the AAA family of adenosine triphosphatase (ATPase) regulates substrate unfolding and translocation. The lid and additional subunits of the base integrate substrate receptors, coordinating the activity of proteasomal deubiquitinating enzymes and transitional states[9,10,13]. The removal of ubiquitin chains from substrates by proteasomal deubiquitylating enzymes is a tightly regulated step in the 26S mechanism[13–16]. In this process, USP14 trims supernumerary ubiquitin chains conjugated in substrates, and, by a sophisticated allostery, controls the steps of ubiquitin recognition, substrate translocation initiation and ubiquitin chain recycling. Notably, USP14-26S proteasomes in exiting conformational states dissociate trimmed ubiquitin slower, causing a delay in substrate reloading[17]. As a consequence, USP14 was initially identified as a delayer of proteasomal activity[15,18]. Additionally, chemical inhibition of USP14 with specific USP14 inhibitors (IU1 compounds)[15,19,20] has an enhancement effect of proteasomal activity[15] In the 26S proteasome mechanism, the process of protein degradation can be viewed as a sequence of events in which ubiquitin tagging of substrates does not play a strictly proteolytic role[9,21,22] Although ubiquitin signaling (i) plays a pivotal role in substrate selection, recruitment, localization, (ii) may assist 26S conformational changes and (iii) promotes the degradation of partially proteolyzed proteins retained in the 26S[23–25]**,** the event that initiates proteasomal degradation is the engagement of a flexible fragment of the substrate by the ATPase engine; this engagement and consequent downstream steps are ubiquitin-independent[9,21,22,26] Indeed, there is evidence of ubiquitin-independent degradation of endogenous and engineered protein substrates by the 26S[27–29] In these cases, the triggers that promote degradation are adaptor factors, affinity surfaces or ligands involved in recruitment and localization of specific substrates[27–31]. From this point of view, the proteasome contains multiple subunits and regions which may act as anchoring sites with a potential in a chimera-based TPD approach[10,13,17,32].

In the present work, by designing small molecule-based chimeras that directly interact with the proteasomal-associated factor USP14 and two model targets, we have developed degraders that target proteins to the 26S in an E3-independent manner[33]. This approach exploits the positioning of USP14 in the RP, and shares similarities with the recently described Rpn1-directed chimeras[34], although in that case the Rpn1 ligands were based on macrocyclic peptides. More recently, degraders using Rpn13 as recruiter have been also reported[35]. In our approach, we chose inosine monophosphate dehydrogenase 2 (IMPDH2), which catalyses a rate-limiting reaction in the *de novo* biosynthesis of guanine nucleotides, essential for the synthesis of RNA and DNA, and defined as a target in leukemias, lymphoma and other types of cancer[35–39]. Moreover, elevated levels of IMPDH2 have been correlated with cancer progression and chemoresistance[37–39]. Nonetheless, only one IMPDH2 degrader has been reported, until now[40]. A second target for degradation was the ceramide transporter CERT1, which conveys ceramides from the endoplasmic reticulum to the Golgi for sphingomyelin (SM) synthesis. By increasing the intracellular levels of ceramides (proapoptotic lipids), CERT1 inhibition sensitizes cancer cells to anti-cancer drugs[41,42], which sustains the interest of developing CERT1-targeted degraders, so far unreported. In light of our data, these 26S-targeting ubiquitin-independent degraders (named "26S-UIDs"[30]) appear as a versatile alternative tool for TPD-drug development (Fig. 1b).

Results

Design and synthesis of chimeras targeting the 26S proteasome regulator USP14

In order to approach a type of small-molecule chimera that binds directly to the 26S with the capacity to promote degradation of native protein substrates, USP14 was considered a good binding candidate owing to the properties offered by this factor. First, USP14 is localized at the base of the RP, interacting with the receptor Rpn1 and establishing contacts with ATPase subunits (Fig. 1a)[17]. Second, USP14 exhibits trimming activity on ubiquitin chains attached to the substrates and adopts positions

ARTICLE IN PRESS

proximal to the ATPase pore (Fig. 1a)[15,17]. Third, USP14 is a complex allosteric regulator of the proteasome and USP14 inhibition enhances 26S activity[15,17]. Moreover, highly selective small molecule inhibitors of USP14 (IU1 and derivatives), exhibit the capacity to increase the activity of the 26S[15,19], and show affinities towards USP14 compatible with their use in a chimera design[15,19,20]. Notably, IU1 compounds have not been explored as chimera ligands yet, with the exception of a recent article[43]. Therefore, we hypothesized that IU1-based chimeras would interact with the proteasome via USP14 and localize targets to a position prone to degradation, bypassing the requirement of previous ubiquitination.

Analysis of the structure of an IU1 optimized version, **IU1-248** (Fig. 1c), bound to USP14 (PDB 6IIN[20]) showed that this ligand has an exposed hydroxyl group (Fig. 2a) that does not seem essential for binding and which is amenable to derivatization, constituting a convenient linker attachment point in the final 26S-UIDs. As for the targets selected (IMPDH2 and CERT1), the structure of IMPDH2 with the bound inhibitor **VX-497**[44] (Fig. 1c) shows that the tetrahydrofuranyl moiety at one end of the molecule is exposed to the solvent and does not establish any significant interaction with the protein (Fig. 2b), thus seeming an appropriate region for linker attachment.

Concerning CERT1, several structures with bound ligands exist in the PDB. A particular family of CERT1 ligands (**HPA** family) that bind to the CERT1-START domain has been described[45]. HPA members contain a polar head that binds deeply in the binding site cavity, and a flexible alkyl chain, which is closer to the surface of the protein (PDB codes 3H3Q, 3H3R, 3H3S and 3H3T[45]). Modeling one of these ligands derivatized with a PEG chain (**HPA-14_PEG$_3$**, Supplementary Fig. 1) suggested that this linker would be exposed to the bulk solvent and it would not perturb the structure of the protein or the binding of the ligand (Fig. 2c). Therefore, these ligands were considered a valid starting point for the design of CERT1-targeting 26S-UIDs.

A preliminary *in silico* study was performed to determine whether the structures of potential 26S-UIDs based on the above could participate on the formation of ternary complexes with USP14 and the respective protein targets. For that purpose, the software workflow PROTAC-Model[46] was used to challenge the structures of three chimeras (**300**, **330** and **329**, containing different linker lengths, Fig. 1c) against the pair USP14/IMPDH2. The results obtained showed that they were compatible with different relative dispositions of the two proteins (Fig. 2d and Supplementary Figs. 2a-c). Furthermore, alignment of the structures of some of these ternary complexes with the structure of USP14 in the context of 26S (PDB 5GJQ[47]) made evident that they could be superposed without showing significant clashes with the closer 26S-partners (Fig. 2e).

Prompted by the above results, the synthesis of 26S-UIDs targeting IMPDH2 and CERT1 was undertaken using **VX-497** and an analog of the HPA-family (**366**) (Fig. 1c and Supplementary Figs. 3 to 12), respectively, as target ligands. At the other end, **IU1-248** was initially chosen as USP14 binder, although we switched to a distinct USP14 binder (i.e. **317**, Fig. 1c) based on the results obtained with the IMPDH2 chimeras (*vide infra*). Each pair of ligands was connected through PEG based linkers conveniently attached to groups mostly exposed to the bulk solvent (Fig. 2a-c).

Functional characterization of 26S-UIDs targeting IMPDH2

Compounds **300**, **329** and **330**, which feature the USP14 inhibitor **IU1-248** and only differ in the PEG linker length (Fig. 1c), were prepared as putative IMPDH2 degraders (Supplementary Figs. 3, 5, 7 and 8).The compounds were first tested as IMPDH2 inhibitors using inosine 5'-monophosphate (IMP) as a substrate (Supplementary Fig. 13) and as USP14 inhibitors in Ub-AMC processing assays[18] (Supplementary Fig. 14). These assays showed that the chimeras containing the **VX-497** and **IU1-248** moieties could inhibit both IMPDH2 and USP14. A quantitative measurement of chimera binding was obtained by SPR, which revealed K_D values for **300, 329** and **330** towards USP14 and IMPDH2 in the 18-36 μM range (Supplementary Table 2 and Supplementary Fig. 15). Together, these results show that chimeras can productively interact with USP14 and IMPDH2 in a functional context, suggesting the feasibility of our approach.

After the above assays in cell-free systems, chimeras were tested in HeLa cells. This cell line was selected after a study reporting that mycophenolic acid, an IMPDH2 selective inhibitor, was more effective at inhibiting cancer cell proliferation in fast-growing

ARTICLE IN PRESS

cell lines, such as HeLa and Caco2, than in slow-growing cells[48], suggesting that HeLa cell viability would be sensitive to IMPDH2 degradation.

Treatments with compounds **300**, **329** and **330** revealed that **300** was able to induce the degradation of IMPDH2 at low μM concentrations, whereas **330** was less potent and **329** was inactive. However, in time-course experiments ranging from 4 h to 96 h, degradation was observed only at long times (72-96 h) after a single treatment with different chimera concentrations (Figs. 3a,b and Supplementary Fig. 16), which denotes a time-consuming process as compared to those reported for E3-based Protacs.

Compound **354** (Fig. 1c) featuring ligand **317**, a derivative of **IU1c**, was also prepared (Supplementary Figs. 4, 5 and 9) and tested as USP14 ligand. In contrast to **IU1-248**, **IU1c** was reported not to inhibit USP14, but its capacity to bind USP14 was not determined[15]. Similar to **IU1c**, **317** and its derivative **352** (Fig. 1c) were also poor USP14 inhibitors (Supplementary Fig. 14), but the final chimera **354** showed a higher capacity to inhibit USP14 (Supplementary Fig. 14). However, quantification of the direct interaction of **354** with USP14 by SPR revealed a K_D value of 11 μM, better than the values corresponding to **IU1-248**-based chimeras **300**, **330** and **329** (18, 30 and 24 μM, respectively, Supplementary Table 2). Furthermore, comparison of the measured K_D of **317** (12 μM) to that of **IU1-248** (13 μM), suggested that the **IU1c** moiety present in **317** could indeed bind to USP14 with similar affinity as **IU1-248**. Therefore, **317** appeared to offer an optimized profile as ligand, exhibiting high affinity but low inhibition towards USP14, properties that are apparently also conferred to its derivative **354**. Computational modeling suggested that compounds **IU1c** and **317** can bind to USP14 at the same site as **IU1-248**, but with an orientation which would pose a lower steric impediment to ubiquitin binding and processing, and which could explain the above experimental observations (*Additional Molecular Modeling Results*, Supplementary Information).

Notably, when **354** was used in HeLa cells, potent IMPDH2 degradation was observed at sub-micromolar range, with a complete depletion of the target at 500-1000 nM (Figs. 3a,b), outperforming **300**. However, like with **300**, IMPDH2 degradation occurred at long incubation times (72-96 h) (Figs. 3a,b and Supplementary Figs. 16a-c,h), at which **354** was still present in the medium as shown by LC/MS analyses (Supplementary Fig. 17). Treatments distributed in multiple additions of **354** did not remarkably change the degradation time pattern (Supplementary Fig. 16i). Of note, in agreement with their mechanisms of action, cell treatments with **354** and **VX-497** caused opposite effects in steady state levels of IMPDH2: whereas **354** decreased or totally depleted IMPDH2, **VX-497** caused a dose-dependent increase of IMPDH2 levels, by a feedback response of the purine synthesis pathway[49–51] (Fig. 3a,b and Supplementary Figs. 16e,g).

Mechanistic studies using proteasome CP blockers (bortezomib and marizomib) were performed in HeLa and in HeLa cells stably overexpressing IMPDH2 (clone 522-4) to counteract toxicity due to IMPDH2 degradation. Indeed, these cells were more resistant to **354** than the parental HeLa cells (Fig. 3c, left). As shown in Fig. 3d, the proteasome inhibitors bortezomib and marizomib rescued IMPDH2 degradation induced by **300** (in HeLa) and by **354** (in 522-4). In the latter case, IMPDH2 overexpression protected cells from massive death, but a higher degrader concentration was required for depletion of the overexpressed protein. Conversely, the E1-Ub activating enzyme inhibitor MLN7243 did not prevent the target degradation (Fig. 3e). Furthermore, IMPDH2 depletion was counteracted dose dependently by preincubation with the IMPDH2 ligands **VX-497** and **352** (Fig. 3f). This effect could only be partially observed since **VX-497** at concentrations higher than 10 μM abrogated cell growth (Fig. 3c, right). These results show that **354** provokes ubiquitination-independent IMPDH2 degradation by interacting with the target and the 26S-proteasome.

To show that IMPDH2 degradation occurs in a USP14-dependent manner, the effect of **354** on IMPDH2 degradation in MEFs *Usp14*$^{-/-}$ versus wild-type was tested. We observed that IMPDH2 degradation was induced in MEFs-WT, whereas in MEFs *Usp14*$^{-/-}$degradation was not only prevented (Fig. 3g), but the IMPDH2/Actin ratios were significantly higher in

ARTICLE IN PRESS

354-treated cells that in controls. This resembles the effect observed with **VX-497** (see above), indicating that in the absence of USP14, the chimera acts as an IMPDH2 inhibitor and IMPDH2 levels increase by a feedback response of the purine synthesis pathway.

In agreement with the involvement of IMPDH2 in favoring cancer progression[52–54], IMPDH2 degrader **354** provoked a reduction in HeLa cell viability, which was significantly higher in WT than in IMPDH2-overexpressing cells (HeLa 522-4), proving the involvement of the target in **354** cytotoxicity (Fig. 3c, left). On the other hand, **VX-497** was less toxic than **354** and the truncated USP14 interactor **352** (Fig. 1c) did not affect cell viability (Fig. 3c, right). Since neither **VX-497** nor **352** induce IMPDH2 degradation, this result supports that **354**-promoted IMPDH2 depletion is involved in cell killing.

Functional characterization of 26S-UIDs targeting CERT1

Having observed good IMPDH2 degradation activity using USP14-directed chimeras, in particular with **354**, and to assess whether long incubation times were required for degradation with USP14-recruited 26S-UIDs, we turned our attention to CERT1, a target in cancer[42]. For that purpose, we considered to use **317** as USP14 ligand to develop a small series of CERT1-targeting 26S-UIDs (**395**, **413**, **386**, **368** and **419)**, leveraging the CERT1 interaction with HPA-antagonist derivatives (Fig. 1c and Supplementary Figs. 10 and 11). Since triple negative breast cancer MDA-MB-231 cells were used by Swanton *et al*. to prove the interest of CERT1 as a therapeutic target in oncology[42], the CERT1-targeting 26S-UIDs were first tested in this cell line. In time course assays, **368** showed a degradation effect in 16-24 h, with a maximum degradation observed at 24 h (Fig. 4a), in contrast with the long treatment times required for IMPDH2 degradation. After 24 h of incubation, dose-dependent degradation of CERT1 was observed for all five compounds, each featuring distinct linker lengths (Figs. 4b,c). To compare their effectiveness as degraders, a two-way ANOVA was performed to assess how CERT1 degradation (quantified via densitometric analysis) varied with 26S-UIDs structure and concentration, treated as independent variables. Post-hoc Tukey's tests indicated that none of the 26S-UIDs induced significantly greater degradation than the others at the concentrations tested (Supplementary Fig. 18). A similar pattern was observed in HER2-positive breast cancer cell lines MDA-MB-453 and BT-474 (Supplementary Fig. 19). However, in these cases, some statistically significant differences emerged at 40 μM for certain compounds, consistent with a potential hook effect (Supplementary Fig. 18). Mechanistic studies showed that the proteasome inhibitor marizomib rescued CERT1 degradation induced by **368** in MDA-MB-453 cells (both used as models), while E1-Ub activating enzyme inhibitor MLN7243 did not prevent CERT1 degradation (Fig. 5a). The accumulation of K48-linked ubiquitinated proteins confirmed proteasome inhibition by marizomib, while the absence of ubiquitinated histone H2A/H2B proved the effectiveness of MLN7243[55] Furthermore, CERT1 depletion was abrogated dose-dependently by preincubation with the CERT1 ligand **366** (Fig. 5b) and the USP14 ligand **352** (Fig. 5c). Additionally, incubations with ligands **317** and **366** did not induce changes on CERT1 levels (Supplementary Fig. 20). Since marizomib did not rescue CERT1 degradation to the control levels, the possibility of induction of autophagosomal degradation of CERT1 by the USP14-based degraders was investigated. To this end, the levels of LC3-II, a hallmark for autophagy, were, determined in MDA-MB-453 treated with **386** in the presence or absence of autophagy inhibitors. As shown in Fig. 5d, **386** induced CERT1 degradation to similar extents in both the absence and the presence of lysosomal protease inhibitors (lanes 3 vs 7), which block the last step of autophagic degradation, leading to accumulation of LC3-II. Moreover, in both cases, marizomib rescued CERT1 degradation to similar levels (lanes 4 vs 8). Similar results were found with chloroquine (Fig. 5e, lanes 3 vs 7 and lanes 4 vs 8), which inhibits the autophagy flux by impairing the autophagosome–lysosome fusion. Overall, these results indicate that CERT1 degradation involves the proteasome and that the contribution of autophagy is negligible. To show that CERT1 degradation is USP14-dependent, **368** effect was tested in MEFs, *Usp14*$^{-/-}$ versus wild-type. It was observed that CERT1 degradation was promoted in MEFs-WT, but not in MEFs *Usp14*$^{-/-}$ (Fig. 5f). These results show that chimeras containing **317** and **366** induce CERT1 degradation by interacting with CERT1 and the 26S-proteasome, in a ubiquitination-independent and USP14-dependent process.

ARTICLE IN PRESS

Since CERT1 transports ceramides from the ER to the Golgi apparatus for SM synthesis, CERT1 degradation was expected to induce an increase in ceramides and a decrease in SM levels. In agreement with the former, treatment of MDA-MB-231 cells with **368** induced an increase in ceramide and this increase was significantly higher for the C14-C20 ceramide species than for the C22-C24 ceramides (Fig. 6a). Similar results were found with **413** in $HER2^+$ MDA-MB-453 cells and with **395** in BT-474 cells (Figs. 6b,c). This is consistent with the report that CERT1 efficiently transfers ceramides having C14, C16, C18, and C20 chains (C14-C20Cers), while longer acyl chains (C22-24Cers) are more poorly transported[58]. Intriguingly, the expected decrease in SM amounts upon treatment was not observed in any cell line (Supplementary Fig. 21), which is likely due to SM replenishment by uptake from the serum present in the cell culture medium.

Modeling of 26S-UIDs ternary complexes

The formation of a USP14/26S-UID/POI ternary complex is the minimal requirement for POI degradation. In order to experimentally validate ternary complex formation, we carried out pulldown assays based on USP14 immobilized on beads, in parallel assessments of IMPDH2 and CERT1 interactions with USP14, in the presence of representative **354** and **386** chimeras. The assays revealed that **354** (1 and 10 μM) or **386** (5 and 30 μM) could induce ternary interactions with both endogenous and recombinant proteins. Control pulldown assays confirmed the specificity of the ternary complex formation. Compounds binding only one protein—**VX-497** (IMPDH2) and **366** (CERT1)— failed to pull down interacting partners, indicating that stable interactions require all three components. Beads lacking USP14 also failed to pull down chimeras or targets, confirming that both did not bind beads unspecifically. Robust pulldown signals were only observed when all components were present, and negative controls further validated interaction specificity (Supplementary Fig. 22).

To elucidate the molecular basis of ternary complex formation, we employed the PROTAC-Model workflow, previously validated for modeling other Protac-mediated assemblies[46]. This approach generates ensembles of structural models grouped into clusters, each ranked according to protein–protein interface energy. Ternary complexes of USP14/IMPDH2 with chimeras **300**, **330**, and **329**—all containing **IU1-248** as the USP14-binding moiety—were modeled as described in the *Computational Methods* section. The simulations yielded 21 models (9 clusters) for **300**, 86 models (11 clusters) for **330**, and 150 models (12 clusters) for **329** (Supplementary Figs. 2a–c). Consistent with previous observations for other Protac systems[58], multiple distinct protein–protein arrangements, rather than a single preferred binding mode, met the conditions of shape complementarity, as well as the geometric and energetic requirements of the chimeras. Remarkably, the lowest-energy cluster for all three 26S-UIDs corresponded to the same overall protein arrangement, suggesting that each chimera can adopt conformations compatible with this configuration (Supplementary Fig. 23a). This arrangement also exhibited the largest buried surface area (Supplementary Fig. 2), indicative of extensive interprotein contacts. Superposition of USP14 from these complexes onto the proteasome-bound USP14 subunit (PDB 5GJQ) revealed that the modeled configurations are sterically compatible with the 26S proteasome, fulfilling a key structural prerequisite for 26S-UID activity (Fig. 2e). Similarly, modeling of the **317**-based chimera (USP14/**354**/IMPDH2) (Supplementary Fig. 2d) produced a top-ranked structure closely resembling that of **300**, with only minor differences in binding geometry (Supplementary Fig. 23a). Ternary complex models were also generated for USP14/CERT1-START bound to chimeras **368, 386, 413, 395,** and **419** (Supplementary Fig. 24). In this case, a broader diversity of binding modes and interaction energies was observed, primarily attributable to differences in PEG–carbamate linker length. Chimeras **368** (3 PEG units), **386** (2 PEG units), and **413** (1 PEG unit) exhibited similar binding modes, whereas **419** (5 PEG units) and **395** (no linker) adopted distinct, less favorable configurations with higher interface energies, particularly pronounced for **395** (Supplementary Figs. 23b). Despite these suboptimal geometries, both chimeras retained potent degrader activity (see previous section), suggesting that degradation efficacy is not strictly dependent on interface energy or complex geometry. Structural analysis of the modeled ternary complexes indicated that stabilization arises from multiple intermolecular interactions between the 26S-UID molecules and their binding partners (Figs. 7a,b), as well as between each pair of proteins (Supplementary Fig.

ARTICLE IN PRESS

25). Notably, high surface complementarity was observed between protein pairs that have not naturally co-evolved to interact. This complementarity is partly explained by the consistent occupation of USP14's concave surface region by the target protein—a region that corresponds to USP14's native ubiquitin-binding site (residues 183–213, 265–278, 294–302, 330–342, and 428–434) (Figs. 7c,d)[46,58].

Discussion

In the present work we have developed a type of proteolytic chimeras (26S-UIDs) that induce degradation by directing targets to the 26S proteasome, using the proteasomal associated factor USP14 as the anchoring site, and evaluated the degradation of two oncologic targets, IMPDH2 and CERT1, as proof-of-concept. Although USP14 exists as a non-proteasomal pool in cells as well[56,57], a very extensive corpus of evidence shows that USP14 mainly functions in the proteasome and that it is strongly activated as a proteasome-bound factor, being virtually inactive as a free form[14,15,17,21,58–61]. Of note, the results shown here recapitulate functional and structural interaction of USP14 with the 26S proteasome, previously characterized by the literature[15,18,28,47]. By taking advantage of the 26S-USP14 association, the 26S-UIDs exploit an unexplored mechanism of action in chimera-induced TPD, based on the localization of non-ubiquitinated targets in proximity to the ATPase motor of the 19S, which has the capacity to engage native protein substrates, unfold and translocate them to the 20S to finally be degraded[9,21,22]. Remarkably, macrocyclic peptides binding to Rpn1 have been recently developed and used to direct protein targets to the 26S for degradation[34]. Even though they are not based on a small molecule ligand, these chimeric compounds represent the first functional validation of the 26S-directed approach. Moreover, chimeras recruiting Rpn13 have been shown to degrade BRD4[62]. In addition, during the revision of the current article, chimeras based on IU1 molecules directed to USP14 have been reported to efficiently degrade histone deacetylase (HDAC) isoforms[43]. As shown in refs. 34 and 35, and in our work, 26S-UIDs do not hijack E3 ligases in order to promote proteasomal signaling of the targets dependent on ubiquitination[1–3]. In order to design our 26S-UIDs, we utilized the IU1 inhibitor family, developed and optimized by groups in the field[15,19,20]. IU1 series exhibit high selectivity as inhibitors of human USP14, and optimal exposure of functionalizing elements when bound in the allosteric pocket of USP14[20] (Figs. 2a-c). Interestingly, herein we have serendipitously discovered that **317**, derivative of compound **IU1c,** acts as a highly efficient ligand for USP14 in the context of a chimera, exhibiting good binding but low inhibition towards USP14, and improved responses with respect to 26S-UIDs based on **IU1-248** (Fig. 3). With this structural configuration, we have approached 26S-UIDs by designing chimeras directed to IMPDH2 and CERT1. The generated constructs were evaluated in cells, in vitro assays and by SPR (Figs. 3 to 6, Supplementary Figs. 13 to 22, 26 and 27, and Supplementary Table 2). In addition, since the starting hypothesis that a minimal requirement for 26S-UID activity is the formation of a ternary complex between USP14/26S-UID/POI (Supplementary Fig. 22), we investigated *in silico* different ternary complexes. The models generated constitute reasonable arrangements of the three components that satisfy the conditions of shape complementarity between proteins, as well as the geometric and energetic requirements of the chimeras (Fig. 7 and Supplementary Figs. 2, 23 and 24). The use of proteasome and Ub-activating enzyme inhibitors evidenced the dependence on proteasomal activity and independence on ubiquitination of 26S-UIDs. Importantly, the USP14-dependence of target degradation was demonstrated in *Usp14*$^{-/-}$ cells, in which degradation of both targets was prevented (Figs. 3g and 5f). Additionally, both targets could be degraded by proteasomal colocalization, with potencies depending on the target and amenable for improvement. Furthermore, the target ligands (**VX-497** and **352** for IMPDH2 and **366** and **352** for CERT1) prevented degradation (Figs. 3f, 5b and 5c), proving the interaction of 26S-UIDs with targets *in cellulo*. Of note, in treatments with **413, 368 and 386** (40 μM) a slight hook effect was observed in different cell lines (Figs. 4b,c and Supplementary Figs. 18 and 19). Since CERT1 is a cytosolic target and cytosolic proteasome is estimated to be less abundant than nuclear proteasome (~170 nM versus ~900 nM[63]), it is likely that both CERT1 and cytosolic proteasomal saturations by chimeras are responsible for the observed effect.

ARTICLE IN PRESS

Treatment times required to achieve degradation were target-dependent. While CERT1 degradation was observed within the 16–24-hour range, IMPDH2 degradation required 72-96 h. MOA-wise, the time-consuming depletion of IMPDH2 is an intriguing observation. However, a possible explanation could be linked to the observed increase in both IMPDH2 mRNA levels, assessed by qPCR (Supplementary Fig. 26) and protein levels (Supplementary Figs. 16c,d,g), induced by **VX-497** and **VX-497**-based compounds (e.gr., **300** and **354**), in the initial 24-48 h of treatment, which may counteract the effect of degradation. An additional explanation could be the kinetics of cellular internalization and response to compounds. The observation that the uptake of **354** was ca. 4 times higher at 96 h than at 24 h (Supplementary Fig. 17), is aligned with a delayed response in IMPDH2 degradation. The quicker transcriptional activation observed (Supplementary Fig. 26) could indicate that binary interactions (IMPDH2-**VX-497** moiety) are initially favored, versus ternary engagements. Further research would be required to validate these hypotheses. It is worth mentioning that proteasome inhibitors, although notably decreasing target degradation, did not reestablish target levels to those observed in the controls (Figs. 3d and 5a,d,e). The fact that USP14 exists in an extraproteasomal pool and that USP14 plays a role in autophagic flux regulation[64,65] makes conceivable the participation of additional proteolytic pathways under certain conditions. In this regard, our studies with the CERT1 degrader **386**, which brought about similar CERT1 depletion in absence and presence of blockers of the autophagic flux (Figs. 5d,e), rules out the participation of autophagy, at least in our experimental conditions.

Remarkably, this work presents degrading chimeras of a protein involved in sphingolipid metabolism. CERT1 is an important target in ceramide signaling and, despite CERT1 inhibitors have been developed, its induced degradation remained unexplored. Thus, our chimeras represent the initial steps in a therapeutic approach based on proteolytic depletion of CERT1. Since many chemotherapeutic agents increase ceramide levels in cells due to increased de novo synthesis of ceramides[66] and CERT1 represents the main exit gate of ceramide from the ER, it is likely that its manipulation will modulate ceramide levels in cells and their response to chemotherapy. In agreement, CERT1 expression was reported to be increased in paclitaxel-resistant ovarian cancer cell lines, suggesting that CERT1 could be a target for chemotherapy-resistant cancers[42]. In another study, increased expression of CERT1 was found in $HER2^+$ versus $HER2^-$ breast cancer specimens and in primary breast cancers of patients receiving adjuvant chemotherapy, where high expression was associated with poor prognosis[67]. Furthermore, using a RNA interference screen, CERT1 was identified as a resistance promoting gene in a number of common chemotherapeutic agents (paclitaxel, doxorubicin, 5-fluorouracil and cisplatin)[68]. In a later clinical study, CERT1 was a sound marker of paclitaxel resistance in patients with triple-negative breast cancer subjected to combined 5-fluorouracil / doxorubicin / cyclophosphamide therapy in the presence or absence of paclitaxel[69]. These overall works support the role of CERT1 in the regulation of drug sensitivity[66] In this study we have found that our 26S-UIDs induce CERT1 degradation resulting in increased ceramide levels. It is intriguing that all five CERT1-targeted 26S-UIDs exhibit similar potency at the tested concentrations. While this might suggest that the linker length does not significantly influence the degradative activity, the role of membrane permeability cannot be ruled out. It's possible that the compounds differ in their intrinsic potency, but these differences may be obscured by variations in cellular permeability. Further experiments to examine the translational impact of the CERT1 degraders reported here are underway. Interestingly, chimeras **395** and **413** at concentrations that reduced cell viability by a 20% induced sensitization to lapatinib in the $HER2^+$ cell lines MDA-MB-453 and BT-474 (Supplementary Fig. 27). Whether this effect is mediated by CERT1 degradation and the molecular mechanisms involved in the sensitization are under investigation. Besides the report of CERT1 degrading chimeras, we herein present 26S-UIDs that target IMPDH2, which has also been scarcely explored in Protac development[40] despite its relevance in oncology.

In summary, in our work an additional class of UIDs that induce degradation by directing targets to the 26S proteasome using USP14 as the anchoring site is reported. A recent work has reported efficient degradation of histone deacetylase (HDAC) isoforms by means of USP14 interaction[43]. Despite Sun *et al*. do not analyze the involvement of the proteasome in HDAC degradation, they provide sound data that strengthens the USP14-approach in TPD. Here, two proof-of-concept targets relevant

ARTICLE IN PRESS

in human cancer, namely IMPDH2 and CERT1, were selected. In both cases, compound **317**, a derivative of compound **IU1c,** acted as a highly efficient ligand for USP14 in the respective degraders. The generated constructs have been characterized in cells, in vitro assays, by SPR and by *in silico* docking studies. Additionally, we provide evidence that targets are degraded by proteasomal colocalization in a ubiquitin-independent manner and that degradation involves the interaction of the ligand with the protein target. Remarkably, this work presents degrading chimeras of a protein involved in sphingolipid metabolism, namely CERT1. We have shown that compounds **395** and **413** induce the accumulation of pro-death lipids ceramides and sensitize $HER2^+$ breast cancer cells to lapatinib. Although confirmation awaits further investigation, these results suggest that the CERT1 degradation induced by the degraders may be involved in the sensitization. Collectively, the USP14-directed UIDs strategy should emerge as a generalizable versatile and robust type of proteolytic chimeras of intracellular targets with applications in both the study of the proteasome and in drug development.

ARTICLE IN PRESS

Methods

Computational Methods

The package Schrödinger Suite 2022-4[70], through its graphical interface Maestro[71], was used to perform most modeling and visualization tasks. The program Macromodel[72] with the OPLS4 force field[73] and GB/SA water solvation conditions[74] were used for energy minimization. The Protein Preparation Wizard[75] included in Maestro was used to prepare protein structures by removing solvent molecules and ions, filling incomplete residues and gaps, adding hydrogens, setting protonation states and running a restrained minimization using the OPLS4 force-field. This preparation protocol was applied to all proteins studied (USP14, IMPDH2 and CERT1), with some variations depending on the case, as next described. Chain A of structure 6IIN[20], including one molecule of inhibitor **IU1-248** bound to an allosteric cavity close to the active site, was used as initial model of USP14. This structure has several gaps (loops 220-239, 334-339 and 378-400) and incompletely defined residues, which are located mostly away from the inhibitor binding site, except for loop 334-339. Thus, the Homology Modeling module of the Schrodinger Suite, with the Energy-based method and default settings, was used to generate a model of the full sequence between residues 101-494 of USP14 with the bound **IU1-248** inhibitor. This structure was also used to dock a molecule of **IU1c** and its derivative **317**, first using the software Glide[76–78] with default settings and then the best poses were redocked with the Induced Fit Docking protocol[79,80] of the Schrodinger Suite. Similarly, chain A of PDB 6UDO[81] was used to obtain a model of the full sequence between residues 12-514 of IMPDH2 with a docked molecule of inhibitor **VX-497**[44].The structure of this inhibitor was then modified to generate a capped version, **VX-497_cap** (Supplementary Fig. 1), that was later used as starting point to model the corresponding ternary complexes (see below). Finally, PDB 2E3Q[45] was used as model of the START domain of CERT1, to which ligand **HPA-14_PEG$_3$** (Supplementary Fig. 1) was docked, as described above. The stability of this complex (**HPA-14_PEG$_3$**/CERT1) was assessed by running a 500 ns molecular dynamics simulation, as described below. This docked ligand was further modified to introduce a triazine group (**HPA-9_trz**, Supplementary Fig. 1) which was later used to model the corresponding chimeras in the ternary complexes with CERT1 and USP14.

Molecular Dynamics of USP14 complexes

Models of ligands **IU1-248**, **IU1c** and **317** docked to USP14 and of **HPA-14_PEG$_3$** docked to CERT1 were submitted to molecular dynamics with the program Desmond 7.2[82,83], as included in the Schrödinger Suite 2022-4, using the OPLS4 force field. Three simulations were performed for each USP14-ligand complex, starting from different docked poses. These systems were set up using the System Builder of the Maestro-Desmond interface[84]. Solutes were placed in the center of a truncated octahedron periodic box that extended 15 Å away from any solute atom, Na^+ and Cl^- ions were added to achieve neutrality and to reach a 150 mM salt concentration, and systems were solvated with TIP3P water molecules. Thus, each simulation system consisted

ARTICLE IN PRESS

of one USP14 monomer and one bound-ligand molecule, 40 chloride and 48/49 sodium ions (depending on ligand protonation state), and approximately 14330 TIP3P waters. The systems were subjected to the default relaxation protocol consisting of: 100 ps Brownian Dynamics at 10 K in the NVT ensemble, with 50 kcal mol^{-1} $Å^{-2}$ restraints on solute heavy atoms; 12 ps molecular dynamics at 10 K (Lagevin thermostat) in the NVT ensemble, keeping the restraints; 12 ps MD at 10 K and 1.0 atm (Lagevin thermostat and barostat) in the NPT ensemble, keeping the restraints; 12 ps MD keeping previous conditions except for temperature of 300 K; 24 ps MD keeping previous conditions but without restraints. Production MD simulations (500 ns, 2 fs timestep) were performed under the same conditions (PBC, NPT ensemble, 300 K and 1.0 bar) using the Nose-Hoover thermostat method[85] with a relaxation time of 1.0 ps and the Martyna-Tobias-Klein barostat method[86] with isotropic coupling and a relaxation time of 2 ps. Integration was carried out with the RESPA integrator[87] using time steps of 2.0, 2.0, and 6.0 fs for the bonded van der Waals and short range and long range electrostatic interactions, respectively. A cut-off of 9.0 Å was applied to van der Waals and short-range electrostatic interactions, while long-range electrostatic interactions were computed using the smooth particle mesh Ewald method with a 10^{-9} Ewald tolerance[88,89]. Bond lengths to hydrogen atoms were constrained using the Shake algorithm[90]. Coordinates were saved every 250 ps, hence 2,000 snapshots (frames) were obtained from each MD run. The Simulation Interactions application included in the Desmond-Maestro interface was used to analyze the simulations results.

Modeling of ternary complexes with 26S-UIDs

Structural models of the ternary complexes of 26S-UIDs (**300**, **330**, **329**, **354**, **368**, **386**, **413**, **395** and **419**) with their corresponding protein partners were generated with the software workflow PROTAC-Model[46]. This software combines FRODOCK[91,92] for local docking under docking site constraints, RosettaDock[93] for structural refinement[94], for modeling the 26S-UIDs conformations, Open Babel[95] for evaluating the 26S-UIDs conformations, AutoDock Vina[96] for assessing the 26S-UIDs binding modes, VoroMQA[97,98] for reranking the protein−protein complexes, and the fraction of common contact (FCC) clustering method[99] to cluster the final results. Briefly, PROTAC-Model starts with the structures of the two proteins, in our case USP14 and IMPDH2 or CERT1, complexed to their respective ligands. In some cases, different conformations of the bound ligands were assayed. These ligand structures must have anchor atoms where the 26S-UID linker can be attached. Thus, in most cases, for the USP14 ligands **IU1-248** and **317**, their hydroxyl group was defined as anchor atom, while for the IMPDH2 and CERT1 ligands the anchor atoms were conveniently defined, as shown in Supplementary Fig. 1 (**VX-497_cap** and **HPA-9_trz**, respectively). Chimera **395** was an exception due to the lack of a PEG-carbamate linker, thus in this case structures **317a** and **HPA-2** (Supplementary Fig. 1) bound to USP14 and CERT1 were used as input for PROTAC-Model. The first step of the protocol was the docking with FRODOCK of the target proteins to USP14, each containing its own bound ligand, using the ligand anchor atoms as docking sites. In this way, about 25,000 complexes were generated for the USP14/IMPDH2 pairs and about 16,000 for USP14/CERT1. These complexes were then filtered, first by removing those where the two binding sites were too distant. Then RDKit was used to model the full 26S-UIDs into the docked conformations, removing those complexes that yielded unreasonable structures. For the remaining ones, the 26S-UIDs energy was calculated using Obenergy, and the models with unfavorable values were removed. A further elimination criterion was that of the Vina score: only those complexes with a Vina energy score lower than 0 kcal/mol were kept. The remaining models were reranked and refiltered by calculating the protein-protein interface energy with VoroMQA (a unit-less value derived from pseudo-energy potentials[97,98]) and discarding those complexes with positive scores. The resulting complexes were clustered with the FCC method and the clusters were ranked by the best model in each cluster. A further refinement was performed by using RosettaDock to construct 400 models from the best structure of each of the clusters previously generated, and reapplying the filtering, reranking and clustering steps as above. Additional details about this protocol can be found in the original publication[46]. In this way, a number of clusters were generated for each of the ternary complexes studied and representative models of each cluster were obtained (Supplementary Figs. 2 and

ARTICLE IN PRESS

22), which were then minimized with MacroModel. Buried protein surface area was calculated for selected ternary complexes with COCOMAPS[100].

Reagents and general methods for synthesis

All chemicals were purchased from commercial sources and used as received unless otherwise noted. Dry solvents, obtained from a PureSolv dispenser and subsequently degassed with inert gas, were used in most reactions. Synthesis grade or HPLC–grade solvents were used for extractions and purifications. Unless otherwise specified all reactions were performed under Ar inert atmosphere. Progression of the reactions was controlled by thin layer chromatography (TLC), using ALUGRAM® SIL G/UV254 (Macherey–Nagel) silica gel pre–coated aluminum sheets (Layer: 0.2 mm, silica gel 60). Compounds were detected by using UV light (λ=254 nm) and a stain solution of phosphomolibdic acid (5.7% in EtOH). Compounds were purified by flash column chromatography, using silica gel (Chromatogel 60 Å, 35–75 μm) as stationary phase. Mobile phases and gradients are specified in each case. ^{1}H and ^{13}C Nuclear Magnetic Resonance spectra were recorded on a Varian – Mercury 400 (^{1}H NMR at 400 MHz and ^{13}C NMR at 100.6 MHz) spectrometer using $CDCl_3$ or CD_3OD as solvent. Chemical shifts of deuterated solvents were used as internal standards. Chemical shifts are given in parts per million (ppm) and coupling constants (*J*) in Hertz (Hz). Splitting patterns have been described as singlet (s), broad singlet (br s), doublet (d), triplet (t), quartet (q), quintuplet (p), multiplet (m), apparent (app) or combinations of these descriptive names. Specific optical rotations were recorded on a digital Perkin–Elmer 34 polarimeter at 25 ºC in a 1-dm 1-mL cell, using a sodium light lamp (λ=589 nm). Specific optical rotation values (*α+D) are expressed in deg–1·cm^3·g–1, and concentrations (c) are reported in g/100 mL of solvent. High–resolution mass spectra were recorded Waters Acquity UPLC system connected to a Waters LCT Premier Orthogonal Accelerated Time of Flight Mass Spectrometer (Waters,Milford, MA, USA) operated in positive electrospray ionisation mode. Samples were analyzed by FIA (Flow Injection Analysis), using ACN/water (70:30) as mobile phase. Samples were analyzed using a 10 μL volume injection. *m/z* ratios are reported as values in atomic mass units. Detailed methods are given in the Supplementary Information.

Cellular and Molecular Biology Methods

Expression and purification of GST-IMPDH2 protein in *E. coli*

In *E.coli*, glutathione S-transferase fusion vector (pGEX4T3) was used to express and purify GST-IMPDH2 (ALI494 vector; see Supplementary Table 1). Bacterial cultures were grown to an OD_{600} of 0.7, induced with 500 μM isopropylthiogalactoside (IPTG) overnight at 16 °C. Cells were harvested, resuspended with 5 volumes of lysis buffer containing 50 mM NaH_2PO_4 pH 7.4, 150 mM NaCl, 5% glycerol and 1X concentration of protease complete inhibitor cocktail EDTA free (Roche), and lysed sonicating with 30% amplitude during 2 effective minutes (10´´ON/15´´OFF). The lysate was clarified at 15000 g for 45 min, filtered using cheese cloth, and the supernatant was applied to Glutathione agarose (Merck) at a ratio of 1 mL beads per 2 gr cell pellet. The binding was done in end-over rotation at 4 ºC for 3 h. Beads were washed with 30 bed volumes of 50 mM NaH_2PO_4 pH 7.4, 150 mM NaCl, 5% glycerol. Proteins were eluted with a reduced glutathione buffer of 50 mM NaH_2PO_4 pH 7.4, 5% glycerol and 30 mM reduced glutathione. Reactions were incubated at 4 ºC overnight. The efficiency of elution was determined by SDS-PAGE and Coomassie Brilliant Blue staining analysis.

Expression and purification of 6His-USP14 protein in *E. coli*

In *E.coli*, 6-His fusion vector (pET28a) was used to express and purify 6His-USP14 (BCO454 vector; see Supplementary Table 1). Bacterial cultures were grown to an OD_{600} of 0.7, induced with 500 μM isopropylthiogalactoside (IPTG) over night at 16 °C. Cells were harvested, resuspended with 5 volumes of lysis buffer containing 50 mM NaH_2PO_4 pH 7.4, 10 mM imidazole, 150 mM NaCl, 5% glycerol and 1X concentration of protease complete inhibitor cocktail EDTA free (Roche), and lysed sonicating with 30% amplitude during 2 effective minutes (10 s ON/15 s OFF). The lysate was clarified at 15000 g for 45 min, filtered using

ARTICLE IN PRESS

cheese cloth, and the supernatant was applied to Ni-NTA beads (Invitrogen) at a ratio of 1 mL of beads per 2 g cell pellet. The binding was done in end-over rotation at 4 ºC for 3 h. Beads were washed with 15 bed volumes of 50 mM NaH_2PO_4 pH 7.4, 25 mM imidazole, 150 mM NaCl, 5% glycerol followed by 15 bed volumes of 50 mM NaH_2PO_4 pH 7.4, 25 mM imidazole, 300 mM NaCl, 5% glycerol. 6His-USP14 protein was eluted with a buffer containing 50 mM NaH_2PO_4 pH 7.4, 200 mM imidazole, 150 mM NaCl, 5% glycerol. The efficiency of elution was determined by SDS-PAGE and Coomassie Brilliant Blue staining analysis.

Ub-AMC processing assays in 26S-USP14

Assays were performed in a buffer containing 50 mM Tris pH 7.4, 1 mg/mL BSA, 1 mM DTT, 1 mM ATP/$MgCl_2$, premixed VS-proteasome/USP14 (Ubiquitin–vinylsulphone [VS] treated 26S proteasome reconstituted with active USP14, with a ratio of 1.25:20 nM final concentration; Ubiquigent). VS blocks the 26S proteasome endogenous DUB activity by forming an adduct with the active site cysteine in DUBs of thiol proteases. In this way, only the USP14 DUB activity is measured in the assays). VS-proteasome/USP14 were mixed with Ub-AMC and chimeras with a final concentration of 0.5 µM and 50 µM respectively. 30 µL of the mix were dispensed into 384-well low volume plates in triplicate. Ub-AMC hydrolysis was measured at Ex380/Em460 using a Tecan Infinite Nano+. Fluorescence intensity was recorded every minute during 40 min.

Inosine monophosphate dehydrogenase activity assays

Activity of recombinant IMPDH2 was measured by means of enzymatic reactions carried out in the presence of 17.5 µg/ml IMPDH2, 1 mM IMP, 2 mM NAD and 5 µM chimeras or ligands. Formation of NAD(H) was recorded for 3 min at 340 nm in quartz cuvettes, in a Jasco V650 spectrophotometer. Three independent assays were performed for each condition.

Surface plasmon resonance (SPR)

The affinities of the synthesized compounds (here referred to as 'analytes') vs. different recombinant proteins were determined using a BIACORE™ T200 from Cytiva. All experiments were performed at 25 °C and data were collected at a rate of 10 Hz. Recombinant proteins [USP14, IMPDH2, and CERT1 (amino acids 347–598; Abcam 95897), here all three referred as to 'ligands'] were immobilized on a CM5 sensor chip series S (Cytiva) using the amine-coupling method described by the manufacturer. In details, USP14 was immobilized in channel 2, IMPDH2 in channel 3 and CERT1 in channel 4, leaving channel 1 empty as reference. The channels were activated with EDC-NHI (at final concentration of 200 mM and 50 mM, respectively) during 7 min, and blocked with ethanolamine-HCl (1M pH 8.5) during the same time, as the activation. For the immobilization, the ligands were diluted with 10 mM sodium acetate buffer at pH 5.0, for USP14 and CERT1, and pH 5.5 for IMPDH2. The density of the coupling was calculated to achieve a theoretical maximum analyte binding capacity (R_{max}) within the range of 20-150 RUs, with an injection time between 50 and 75 seconds depending on the ligand. The running buffer during the immobilization was PBS with 0.05% Tween20 at a flow rate of 15 µL min^{-1} and 5 µl min^{-1} for the injection of the ligand. The analyses of the analytes binding to the ligands were performed in buffer PBS with 0.05% Tween 20 and 5% DMSO at a flow rate of 60 µL min^{-1}. Each of the synthesized compounds was injected in the running buffer over the immobilized USP14, IMPDH2 or CERT1. For all analytes, samples at 100 µM concentration, and a 2-fold dilution series to 6.25 µM concentration, were injected, by duplicates (1,1; 2,2; 3,3; etc.), for 60 s in the association phase, which is followed by 360 s of dissociation phase. Equilibrium-based affinity analysis was performed using report points set 10 s before the end of the injection, within a 5-s window frame. Data were analyzed using Biacore T200 Evaluation Software v3.1 (Cytiva). In brief: (1) solvent correction was applied, (2) the sensorgrams were double-referenced, and (3) a 1:1 steady state affinity model was applied selecting KD fit global, R_{max} and offset fit local.

Generation of IMPDH2-GFP-overexpressing HeLa cells (clone 522-4)

ARTICLE IN PRESS

In order to generate cell lines expressing stable IMPDH2-GFP, HEK293T cells were transfected with the vector BC522 (Cilantro2-IMPDH2), which contain LTR sequences that facilitate the integration of the vector into the host genome, along with the vectors necessary to create the viral particles (vectors BC512, BC513, BC514; see Supplementary Table 1). After 48 hours, medium with the viral particles was collected and transferred to HeLa cells for infection. This process was repeated 72 hours post-transfection. HeLa cells were cultured with the medium with the viral particles for 48 hours, when the medium was changed. After 24 hours, puromycin was added to the medium, and cells were kept growing with antibiotic during the following days. The cells were observed under the microscope to evaluate the fluorescence levels by GFP and, after 8 days, single cell sorting was done, on 96-well plates, using a BD FacsAria Fusion cell sorter (Beckton Dickinson, San Jose, California), using the BD FACSDiva software version 8.0.1. Live cells were gated using DAPI. The cells were cultured until they grew enough to obtain a protein extract to perform a western blot and check IMPDH2-GFP expression.

Cell cultures

HeLa and MDA-MB-231 cell lines and MEFs were grown in DMEM media (Thermo Fisher) supplemented with 10% fetal bovine serum (FBS) (Thermo Fisher), 2 mM L-glutamine (Thermo Fisher) and 100 U/mL penicillin/100 µg/mL streptomycin (Thermo Fisher). MDA-MB-453 and BT-474 cells were grown in DMEM/F12 media (Gibco) supplemented with 10% fetal bovine serum (FBS) (Thermo Fisher), 2 mM L-glutamine (Thermo Fisher), amphotericin B 2.5 µg/mL (Gibco), 100 U/mL penicillin/100 µg/mL streptomycin (Thermo Fisher) and, only with the BT-474 cell lines, 10 µg/ml insulin (Merck) were added. IMPDH2 degradation experiments were performed in media containing 5% FBS.

Cell treatments

For **IMPDH2** degradation assays, HeLa cells were seeded in 6 well-plates at 150000 cells/mL (HeLa cells and wild type or *Usp14*$^{-/-}$ MEFs). 26S-UIDs at the indicated final concentrations were added from stock DMSO solutions 24 h after seeding and cells were collected at the specified times in the figure legends. In mechanistic studies, bortezomib (Signalway Antibody) and marizomib (MedChemExpress) were added 16 h before cell collection (80 h after 26S-UID addition), while MLN7243 (Selleckchem) was added 8 h before cell harvest (64 h after 26S-UID addition). At the specified times of treatment, both adhered (trypsinizaton) and floating cells were collected and processed for WB analysis. For **CERT1** degradation assays (WB protein analysis) and lipidomics, cells were seeded in 6 well-plates at 200000 cells/mL (MDA-MB-231), 250000 cells/mL (MEF) 300000 cells/mL (MDA-MB-453 cell line) or 400000 cells/mL (BT-474 cell line). 26S-UIDs at the indicated final concentrations were added from stock DMSO solutions (10 mM) 24 h (MEF cells) or 48 h (MDA-MB-231, MDA-MB-453 and BT-474 cell lines) after seeding. In experiments with lapatinib (Selleckchem), the drug was added together with 26S-UIDs. In experiments with marizomib (MedChemExpress), cells were preincubated for 3 h with the inhibitor, the medium was removedand fresh medium containing 26S-UIDs at the concentrations shown was added. In experiments with MLN7243 (Selleckchem) and competitor ligands (**366** and **352**), the compounds were added 3 h prior addition of 26S-UIDs to the cells. DMSO was added as control in all cases. In experiments to assess the role of autophagy in CERT1 degradation, proteasome inhibitors (PI, which contain E64D, 5 µg/mL and pepstatin A, 5 µg/mL) were added together with marizomib and then again with the CERT1 degrader after medium renewal. In the case of chloroquine (Chl), it was added 4 h before cells collection. At the specified times of treatment, both adhered (trypsinizaton) and floating cells were collected and processed for WB analysis or lipidomics. For cell viability determination, cells were plated at a density of: HeLa, 10000 cells/mL; MDA-MB-453, 100000 cells/mL and BT-474, 35000 cells/mL in a 96-well plate and allowed to adhere for 24 h (HeLa cells), 48 h (MDA-MB-231 cells and MDA-MB-453 cells) or 72 h (BT-474 cells). Then cells were treated (single addition) with the indicated doses of compounds for the specified times. Lapatinib was added together with 26S-UIDs Detailed schematic representations of all the assays performed is found in Supplementary Fig.28.

ARTICLE IN PRESS

Cell viability analysis

After the treatments, the MTT reagent (Sigma) was added to the cell culture media and absorbance at 570 nm was quantified after 3 h incubation with a SYNERGY H1 Absorbance microplate reader (BioTek). In Fig. 3**c**, curves adjustment with the four-parameter logistic equation (variable slope) (GraphPad Prism 8, version 8.0.2) afforded the following CC_{50} values (95% Confidence Intervals). In Fig. 3c, **left**: **354**: 1.19 µM (0.61 to 2.32 µM) in parental HeLa; 34.5 µM (12.61 to 94.19 µM) in clone 522-4; in Fig. 3c**, right: 354**: 3.9 µM (1.68 to 9.37 µM); **VX-497**: 11.5 µM (4.15 to 32.15 µM); **352**: > 100 µM.

Protein analysis

Cell pellets were resuspended in the appropriate volume of a 0.25 M saccharose solution. The suspension was submitted to three cycles of 5 s sonication (probe)/5 s resting on ice. The cell lysate was centrifuged at 2500 g for 5 min. The supernatant was collected and protein concentration was determined (BSA as a standard) using a BCA protein determination kit (Thermo Scientific) according to the manufacturer's instructions.

Samples were loaded onto a 10% polyacrylamide gel, separated by electrophoresis at 100 V/2.5-3.0 h and transferred onto a PVDF membrane (100 V/2 h). Unspecific binding sites were then blocked with 5% milk in TBST. Anti-LC3 (Ab48394), anti-IMPDH2 (Ab131158-1001), anti-CERT (Ab72536-1001), anti-USP14 (CS-11931), anti-GAPDH (SC47724), anti-K-48 polyubiquitin (CS-8081) and anti-H2B-Ub (CS-5546) antibodies were diluted 1:1000 in 5% milk in TBST. Anti-actin antibody (Ab5694) was diluted 1:2000 in 5% milk in TBST. Membranes were incubated overnight at 4 ºC under gentle agitation. After washing with TBST, membranes were probed with the correspondent secondary antibody for 1 h at room temperature (IMPDH2, LC3, CERT, K-48 polyubiquitin, H2B-Ub and USP-14: anti-rabbit [NA934V], diluted 1:10000 in 5% milk in TBST; Actin and GAPDH: anti-mouse [170-6516], diluted 1:10000 in 5% milk in TBST). Antibody excess was eliminated by washing with TBST and protein detection was carried out using ECL and membrane scanning with LI-COR C-DiGit® Blot Scanner. Band intensities were quantified by LI-COR Image Studio Lite Software.

Lipidomics

Sphingolipid extracts, fortified with internal standards (N-dodecanoylsphingosine, N-dodecanoylglucosylsphingosine, and N-dodecanoylsphingosylphosphorylcholine, 0.5 nmol each), were prepared by mixing 100 µL of cell lysates with 0.75 mL of methanol and chloroform (2:1 v/v) containing 0.01% BHT. The samples were sonicated in a bath-type sonicator until evenly dispersed, then incubated overnight at 48°C in a water bath. After cooling, 75 µL of 1M KOH in methanol was added, and the samples were sonicated and incubated for 2 hours at 37°C. Solvents were removed using a SpeedVac concentrator, and the samples were redissolved in methanol and transferred to a new tube. Solvents were removed again with the SpeedVac concentrator. The dried samples were redissolved in methanol, centrifuged, and the supernatants were transferred to a glass vial for UPLC analysis.

Liquid chromatography-mass spectrometry was performed using a Waters Acquity Premier UPLC system coupled to a SELECT SERIES Cyclic IMS, which combines a Q-Tof (Quadrupole-Time of Flight) mass spectrometer with cIM (Cyclic Ion Mobility) (Waters, Milford, MA), operated in positive electrospray ionization mode. Full scan spectra from 50 to 1200 Da were acquired, and individual spectra were summed to generate data points every 0.5 s. Mass accuracy and reproducibility were maintained using an independent reference spray via the LockSpray interference. The analytical column was a 100 mm × 2.1 mm i.d., 1.7 µm C8 Acquity UPLC BEH column (Waters). The data was analyzed using MassLynx v4.2 (Waters). The two mobile phases were: phase A: water with 2 mM ammonium formate; phase B: methanol with 1 mM ammonium formate, both containing 0.2% formic acid. A linear gradient was programmed as follows: 0.0 min: 80% B; 3 min: 90% B; 6 min: 90% B; 15 min: 99% B; 18 min: 99% B; 20 min: 80% B; 22 min: 80% B. The flow rate was 0.3 mL/min, and the column was held at 30°C. Quantification was

ARTICLE IN PRESS

performed using the extracted ion chromatogram of each compound with 50 mDa windows. The linear dynamic range was determined by injecting standard mixtures. Positive identification of compounds was based on accurate mass measurement with an error of <5 ppm and their LC retention time, compared to that of a standard.

Analysis of 354 by UPLC-MS

HeLa cells were seeded at the appropriate density to collect $1x10^6$ cells per sample at the end of the experiment and allowed to adhere for 24 h. Then, **354** was added (1 µL of a 10 mM stock solution in DMSO; 10 µM final concentration, 10 nmol). 24 or 96 h after **354**'s addition, the media (containing floating cells) was collected and centrifuged (9000 g, 3 min). Media and pelleted cells were separated. Adhered cells were trypsinized, mixed with the pelleted cells from the media, counted, centrifuged, washed with PBS and spun down again. Pelleted cells were extracted with acetonitrile (300 µL per million cells), sonicated and analyzed by LC/MS as indicated in the previous section. Two-hundred µL of media were diluted with 800 µL of MeOH and kept at 4 °C overnight to precipitate proteins. Then the suspension was centrifuged (9000 g, 3 min) and the supernatant was evaporated under vacuum. The residue was dissolved in 150 µL of acetonitrile, sonicated, centrifuged (9000 g, 3 min) and the supernatant (150 µL) was injected into the mass spectrometer after addition of 200 pmol of C17-sphinganine as internal standard.

Pull-down assays

Immobilized His-USP14 was obtained as described above in "Expression and purification of 6His-USP14 protein in *E. coli.*" methods, avoiding the elution step. After His-USP14 immobilization, beads were washed thrice with 50 mM NaH_2PO_4, 100 mM NaCl, pH 8 buffer and then incubated in blocking buffer (10% BSA in 50 mM NaH_2PO_4, 100 mM NaCl, pH 8 buffer) for one hour at room temperature. The beads were then washed again thrice with 50 mM NaH_2PO_4, 100 mM NaCl, pH 8 buffer and once with washing buffer (50 mM NaH_2PO_4, 100 mM NaCl, 1 mM DTT, 10% Glycerol, protease inhibitor cocktail, pH 7.5). Empty Ni-NTA control beads were washed and blocked with BSA in the same manner. Then, purified GST-IMPDH2 (see above) or CERT1 (95897 Abcam; digested with enterokinase to remove the His-tag; see below) proteins were added at 500nM final concentration. The beads-substrate mixture was then aliquoted to separate tubes and **386**, **366**, **354** or **VX497** were added at the indicated concentration and incubated at 4ºC for two hours. The beads were washed thrice with 10 column volumes of washing buffer and then eluted with SDS loading buffer.

For experiments in which the input substrate is a whole cell extract (WCE), the sample was prepared as follows. Ten 100 mm dishes of confluent HeLa cells were washed with TBS and then scraped into a 15 mL falcon tube. The cells were pelleted, resuspended in wash buffer, and then lysed by sonication (Branson sonicator microtip, 30% amplitude, 3 cycles of 1 effective minute (3 s ON/3 s OFF). The lysate was cleared by centrifugation and then added to the beads as an input substrate, as above. The digestion of His-CERT1 (95897 Abcam) with enterokinase, in order to remove the His-tag, was carried out as follows: His-CERT1 protein (supplied in 20 mM Tris HCl pH 8, NaCl 100 mM by the manufacturer) was incubated during 16 hours at 22ºC with enterokinase (His-tagged; GenScript, Z03004-100), added in a 1.2 units of EK/10 ug of protein substrate ratio. Released His-tag and His-enterokinase were removed by adding 5 µL Ni-NTA beads in 100 µL protein solution, 2 hours of incubation at 4°C followed by centrifugation. In Suppl. Fig. 22, western blots were detected with: panel A, anti-CERT (Ab72536-1001); Panel B, anti-CERT (PA5-90421); Panels C and D, anti-IMPDH2 (Ab131158-1001); All panels, anti-USP14 (CS-11931).

RNA extraction and reverse transcriptase (RT)-qPCR

Total RNA was extracted using the NZY Total RNA Isolation Kit (NZYtech). Then, cDNA was generated from 100 ng of RNA using the SuperScript® VILO™ (Invitrogen). Gene products were analyzed by qPCR, using NZYSupreme qPCT Green Master Mix 2x (NZYtech) and specific oligonucleotides in a QuantStudio5 machine (AppliedBioSystems), running in the QuantStudio™ Design & Analysis Software (AppliedBioSystems). Each value was corrected by human Actine and represented as relative units.

ARTICLE IN PRESS

Each experiment was performed in duplicate. qPCR oligonucleotide sequences used, are: IMPDH2 forward: 5'-GTGAAGCTGACAAAATCAAAGTGGC-3'**,** IMPDH2 reverse: 5'-CTCTGGGCACCAATGTCCTGGC-3'**,** Actin forward: 5'-CACCATTGGCAATGAGCGGTT-3'**,** Actin reverse: 5'-AGGTCTTTGCGGATGTCCACGT-3'.

Data availability

Supporting computational and chemical methods (including compound synthesis and NMR spectra) are described in the supplementary file, which also includes Supplementary molecular modeling results, supplementary tables, figures, movies, PDB-formatted files. The raw data generated in this study are provided in the Supplementary Source Data file. The computational source data can be accessed at https://doi.org/10.5281/zenodo.18313893. Source data are provided with this paper.

References

1. Pettersson, M. & Crews, C. M. PROteolysis TArgeting Chimeras (PROTACs) — Past, present and future. *Drug Discov. Today Technol.* **31**, 15–27 (2019).
2. Verma, R., Mohl, D. & Deshaies, R. J. Harnessing the Power of Proteolysis for Targeted Protein Inactivation. *Mol. Cell* **77**, 446–460 (2020).
3. Lee, J. *et al.* Discovery of E3 Ligase Ligands for Target Protein Degradation. *Molecules* **27**, 6515 (2022).
4. Cai, H., Zhang, T. & Hu, Y. Global landscape of PROTAC: Perspectives from patents, drug pipelines, clinical trials, and licensing transactions. *Eur. J. Med. Chem.* **299**, 118055 (2025).
5. Petrilli, W. L. *et al.* From Screening to Targeted Degradation: Strategies for the Discovery and Optimization of Small Molecule Ligands for PCSK9. *Cell Chem. Biol.* **27**, 32--40.e3 (2020).
6. Lai, A. C. *et al.* Modular PROTAC Design for the Degradation of Oncogenic BCR-ABL. *Angewandte Chemie International Edition* **55**, 807–810 (2016).
7. Ottis, P. & Crews, C. M. Proteolysis-Targeting Chimeras: Induced Protein Degradation as a Therapeutic Strategy. https://doi.org/10.1021/acschembio.6b01068 (2017) doi:10.1021/acschembio.6b01068.
8. Gustafson, J. L. *et al.* Small-Molecule-Mediated Degradation of the Androgen Receptor through Hydrophobic Tagging. *Angewandte Chemie - International Edition* **54**, 9659–9662 (2015).
9. Dong, Y. *et al.* Cryo-EM structures and dynamics of substrate-engaged human 26S proteasome. *Nature* **565**, 49–55 (2019).
10. Lander, G. C. *et al.* Complete subunit architecture of the proteasome regulatory particle. *Nature* **482**, 186–191 (2012).
11. Glickman, M. H. *et al.* A Subcomplex of the Proteasome Regulatory Particle Required for Ubiquitin-Conjugate Degradation and Related to the COP9-Signalosome and eIF3. *Cell* **94**, 615–623 (1998).
12. Groll, M. *et al.* Structure of 20S proteasome from yeast at 2.4 A resolution. *Nature* **386**, 463–471 (1997).
13. Verma, R. *et al.* Role of Rpn11 metalloprotease in deubiquitination and degradation by the 26S proteasome. *Science* **298**, 611–615 (2002).
14. Lee, B.-H. *et al.* USP14 deubiquitinates proteasome-bound substrates that are ubiquitinated at multiple sites. *Nature* **532**, 398–401 (2016).
15. Lee, B.-H. *et al.* Enhancement of proteasome activity by a small-molecule inhibitor of USP14. *Nature* **467**, 179–184 (2010).
16. Yao, T. *et al.* Proteasome recruitment and activation of the Uch37 deubiquitinating enzyme by Adrm1. *Nat. Cell Biol.* **8**, 994–1002 (2006).
17. Zhang, S. *et al.* USP14-regulated allostery of the human proteasome by time-resolved cryo-EM. *Nature* **605**, 567–574 (2022).
18. Hanna, J. *et al.* Deubiquitinating enzyme Ubp6 functions noncatalytically to delay proteasomal degradation. *Cell* **127**, 99–111 (2006).
19. Boselli, M. *et al.* An inhibitor of the proteasomal deubiquitinating enzyme USP14 induces tau elimination in cultured neurons. *Journal of Biological Chemistry* **292**, 19209–19225 (2017).
20. Wang, Y. *et al.* Small molecule inhibitors reveal allosteric regulation of USP14 via steric blockade. *Cell Res.* **28**, 1186–1194 (2018).
21. Bard, J. A. M., Bashore, C., Dong, K. C. & Martin, A. The 26S Proteasome Utilizes a Kinetic Gateway to Prioritize Substrate Degradation. *Cell* **177**, 286-298.e15 (2019).
22. de la Peña, A. H., Goodall, E. A., Gates, S. N., Lander, G. C. & Martin, A. Substrate-engaged 26S proteasome structures reveal mechanisms for ATP-hydrolysis-driven translocation. *Science* **362**, (2018).
23. Chu, B. W. *et al.* The E3 ubiquitin ligase UBE3C enhances proteasome processivity by ubiquitinating partially proteolyzed substrates. *J. Biol. Chem.* **288**, 34575–34587 (2013).
24. Gottlieb, C. D., Thompson, A. C. S., Ordureau, A., Harper, J. W. & Kopito, R. R. Acute unfolding of a single protein immediately stimulates recruitment of ubiquitin protein ligase E3C (UBE3C) to 26S proteasomes. *J. Biol. Chem.* **294**, 16511–16524 (2019).

ARTICLE IN PRESS

ARTICLE IN PRESS

25. Ding, Z. *et al.* Structural Snapshots of 26S Proteasome Reveal Tetraubiquitin-Induced Conformations. *Mol. Cell* **73**, 1150-1161.e6 (2019).
26. Prakash, S., Tian, L., Ratliff, K. S., Lehotzky, R. E. & Matouschek, A. An unstructured initiation site is required for efficient proteasome-mediated degradation. *Nat. Struct. Mol. Biol.* **11**, 830–837 (2004).
27. Erales, J. & Coffino, P. Ubiquitin-independent proteasomal degradation. *Biochim. Biophys. Acta* **1843**, 216–221 (2014).
28. Bashore, C. *et al.* Ubp6 deubiquitinase controls conformational dynamics and substrate degradation of the 26S proteasome. *Nat. Struct. Mol. Biol.* **22**, 712–719 (2015).
29. Janse, D. M., Crosas, B., Finley, D. & Church, G. M. Localization to the proteasome is sufficient for degradation. *J. Biol. Chem.* **279**, 21415–21420 (2004).
30. Balzarini, M. *et al.* Chemically Induced Degradation of Native Proteins by Direct Recruitment to the 26S Proteasome. *bioRxiv* 2023.07.19.549534 (2023) doi:10.1101/2023.07.19.549534.
31. Ma, Y., Xu, J., Huang, P., Bai, X. & Gao, H. Ubiquitin-independent, Proteasome-mediated targeted degradation of KRAS in pancreatic adenocarcinoma cells using an engineered ornithine decarboxylase/antizyme system. *IUBMB Life* **71**, 57–65 (2019).
32. Husnjak, K. *et al.* Proteasome subunit Rpn13 is a novel ubiquitin receptor. *Nature* **453**, 481–488 (2008).
33. Testa, A., Hughes, S., Butcher, S. P. & Ciulli, Alessio. Preparation of bifunctional molecules for targeting Usp14. *PCT Int. Appl.* 279pp. (2019).
34. Bashore, C. *et al.* Targeted degradation via direct 26S proteasome recruitment. *Nat. Chem. Biol.* **19**, 55–63 (2023).
35. Liu, X. *et al.* IMPDH inhibition activates TLR-VCAM1 pathway and suppresses the development of MLL-fusion leukemia. *EMBO Mol. Med.* **15**, e15631 (2023).
36. Tzoneva, G. *et al.* Clonal evolution mechanisms in NT5C2 mutant-relapsed acute lymphoblastic leukaemia. *Nature* **553**, 511–514 (2018).
37. Li, H.-X. *et al.* IMPDH2 mediate radioresistance and chemoresistance in osteosarcoma cells. *Eur. Rev. Med. Pharmacol. Sci.* **18**, 3038–3044 (2014).
38. He, Y. *et al.* Over-expression of IMPDH2 is associated with tumor progression and poor prognosis in hepatocellular carcinoma. *Am. J. Cancer Res.* **8**, 1604–1614 (2018).
39. Tian, Y., Zhang, J., Chen, L. & Zhang, X. The expression and prognostic role of IMPDH2 in ovarian cancer. *Ann. Diagn. Pathol.* **46**, 151511 (2020).
40. Sohbati, H., Amini, M. & Balalaie, S. Synthesis and Biological Evaluation of Novel Anti-leukemia Proteolysis-Targeting Chimeras in Degradating Inosine Monophosphate Dehydrogenase. *Iran. J. Pharm. Res.* **21**, e129251 (2022).
41. Chung, L. H., Liu, D., Liu, X. T. & Qi, Y. Ceramide Transfer Protein (CERT): An Overlooked Molecular Player in Cancer. *Int. J. Mol. Sci.* **22**, (2021).
42. Swanton, C. *et al.* Regulators of mitotic arrest and ceramide metabolism are determinants of sensitivity to paclitaxel and other chemotherapeutic drugs. *Cancer Cell* **11**, 498–512 (2007).
43. Sun, T. *et al.* Targeted Degradation of Histone Deacetylases via Bypassing E3 Ligase Targeting Chimeras (BYETACs). *ACS Med. Chem. Lett.* **16**, 1155–1162 (2025).
44. Sintchak, M. D. & Nimmesgern, E. The structure of inosine 5'-monophosphate dehydrogenase and the design of novel inhibitors. *Immunopharmacology* **47**, 163–184 (2000).
45. Kudo, N. *et al.* Crystal structures of the CERT START domain with inhibitors provide insights into the mechanism of ceramide transfer. *J. Mol. Biol.* **396**, 245–251 (2010).
46. Weng, G., Li, D., Kang, Y. & Hou, T. Integrative Modeling of PROTAC-Mediated Ternary Complexes. *J. Med. Chem.* **64**, 16271–16281 (2021).
47. Huang, X., Luan, B., Wu, J. & Shi, Y. An atomic structure of the human 26S proteasome. *Nat. Struct. Mol. Biol.* **23**, 778–785 (2016).
48. Chen, K. *et al.* Differential Sensitivities of Fast- and Slow-Cycling Cancer Cells to Inosine Monophosphate Dehydrogenase 2 Inhibition by Mycophenolic Acid. *Molecular Medicine* **21**, 792–802 (2015).
49. Chiarelli, L. R. *et al.* Inosine monophosphate dehydrogenase variability in renal transplant patients on long-term mycophenolate mofetil therapy. *Br. J. Clin. Pharmacol.* **69**, 38–50 (2010).
50. Jain, J. *et al.* Regulation of inosine monophosphate dehydrogenase type I and type II isoforms in human lymphocytes. *Biochem. Pharmacol.* **67**, 767–776 (2004).
51. Sanquer, S. *et al.* Induction of inosine monophosphate dehydrogenase activity after long-term treatment with mycophenolate mofetil. *Clin. Pharmacol. Ther.* **65**, 640–648 (1999).
52. Zhou, W. *et al.* Purine metabolism regulates DNA repair and therapy resistance in glioblastoma. *Nat. Commun.* **11**, 3811 (2020).
53. Liu, C.-J. *et al.* The Role of Purine Metabolism-Related Genes PPAT and IMPDH1 in the Carcinogenesis of Intrahepatic Cholangiocarcinoma Based on Metabonomic and Bioinformatic Analyses. *J. Oncol.* **2023**, 5141836 (2023).
54. Huang, Y. *et al.* Wnt/β-catenin signalling activates IMPDH2-mediated purine metabolism to facilitate oxaliplatin resistance by inhibiting caspase-dependent apoptosis in colorectal cancer. *J. Transl. Med.* **22**, 133 (2024).
55. Mamrosh, J. L. *et al.* Quantitative measurement of the requirement of diverse protein degradation pathways in MHC class I peptide presentation. *Sci. Adv.* **9**, eade7890 (2024).
56. Koulich, E., Li, X. & DeMartino, G. N. Relative Structural and Functional Roles of Multiple Deubiquitylating Proteins Associated with Mammalian 26S Proteasome. *Mol. Biol. Cell* **19**, 1072–1082 (2007).
57. Hu, M. *et al.* Structure and mechanisms of the proteasome-associated deubiquitinating enzyme USP14. *EMBO J.* **24**, 3747–3756 (2005).

ARTICLE IN PRESS

ARTICLE IN PRESS

58. Borodovsky, A. *et al.* A novel active site-directed probe specific for deubiquitylating enzymes reveals proteasome association of USP14. *EMBO J.* **20**, 5187–5196 (2001).
59. Leggett, D. S. *et al.* Multiple associated proteins regulate proteasome structure and function. *Mol. Cell* **10**, 495–507 (2002).
60. Crimmins, S. *et al.* Transgenic rescue of ataxia mice with neuronal-specific expression of ubiquitin-specific protease 14. *J. Neurosci.* **26**, 11423–11431 (2006).
61. Catic, A. *et al.* Screen for ISG15-crossreactive deubiquitinases. *PLoS One* **2**, e679 (2007).
62. Ali, E. M. H., Loy, C. A. & Trader, D. J. ByeTAC: Bypassing an E3 Ligase for Targeted Protein Degradation. *bioRxiv : the preprint server for biology* Preprint at https://doi.org/10.1101/2024.01.20.576376 (2024).
63. Pack, C.-G. *et al.* Quantitative live-cell imaging reveals spatio-temporal dynamics and cytoplasmic assembly of the 26S proteasome. *Nat. Commun.* **5**, 3396 (2014).
64. Kim, E. *et al.* Dual Function of USP14 Deubiquitinase in Cellular Proteasomal Activity and Autophagic Flux. *Cell Rep.* **24**, 732–743 (2018).
65. Xu, D. *et al.* USP14 regulates autophagy by suppressing K63 ubiquitination of Beclin 1. *Genes Dev.* **30**, 1718–1730 (2016).
66. Hajj, C., Becker, A. & Haimovitz-Friedman, A. Novel mechanisms of action of classical chemotherapeutic agents on sphingolipid pathways. *Biol. Chem.* **396**, 669–79 (2015).
67. Lee, A. J. X. *et al.* CERT depletion predicts chemotherapy benefit and mediates cytotoxic and polyploid-specific cancer cell death through autophagy induction. *Journal of Pathology* **226**, 482–494 (2012).
68. Swanton, C. *et al.* Regulators of Mitotic Arrest and Ceramide Metabolism Are Determinants of Sensitivity to Paclitaxel and Other Chemotherapeutic Drugs. *Cancer Cell* **11**, 498–512 (2007).
69. Juul, N. *et al.* Assessment of an RNA interference screen-derived mitotic and ceramide pathway metagene as a predictor of response to neoadjuvant paclitaxel for primary triple-negative breast cancer: A retrospective analysis of five clinical trials. *Lancet Oncol.* **11**, 358–365 (2010).
70. Schrödinger. Release 2022-4. Preprint at (2022).
71. 2022-4, S. R. Maestro, version 13.4. Preprint at (2022).
72. 2022-4, S. R. MacroModel, version 13.8. Preprint at (2022).
73. Lu, C. *et al.* OPLS4: Improving force field accuracy on challenging regimes of chemical space. *J. Chem. Theory Comput.* **17**, 4291–4300 (2021).
74. Still, W. C., Tempczyk, A., Hawley, R. C. & Hendrickson, T. Semianalytical treatment of solvation for molecular mechanics and dynamics. *J. Am. Chem. Soc.* **112**, 6127–6129 (1990).
75. 2022-4, S. R. Protein Preparation Wizard 2022-4. Preprint at (2022).
76. 2022-4, S. R. Glide, version 9.7. Preprint at (2022).
77. Friesner, R. A. *et al.* Glide: a new approach for rapid, accurate docking and scoring. 1. Method and assessment of docking accuracy. *J Med Chem* **47**, 1739–1749 (2004).
78. Halgren, T. A. *et al.* Glide: a new approach for rapid, accurate docking and scoring. 2. Enrichment factors in database screening. *J Med Chem* **47**, 1750–1759 (2004).
79. Schrödinger. Release 2022-4: Induced Fit Docking Protocol. Preprint at (2022).
80. Sherman, W., Day, T., Jacobson, M. P., Friesner, R. A. & Farid, R. Novel procedure for modeling ligand/receptor induced fit effects. *J Med Chem* **49**, 534–553 (2006).
81. Johnson, M. C. & Kollman, J. M. Cryo-EM structures demonstrate human IMPDH2 filament assembly tunes allosteric regulation. *Elife* **9**, (2020).
82. Bowers, K. J. *et al.* Scalable Algorithms for Molecular Dynamics Simulations on Commodity Clusters. in *Proceedings of the ACM/IEEE Conference on Supercomputing (SC06)* (Tampa, Florida, 2006).
83. 2022-4, S. R. Desmond Molecular Dynamics System. Preprint at (2022).
84. 2022-4, S. R. Maestro-Desmond Interoperability Tools. Preprint at (2021).
85. Martyna, G. J., Klein, M. L. & Tuckerman, M. Nosé–Hoover chains: The canonical ensemble via continuous dynamics. *J. Chem. Phys.* **97**, 2635–2643 (1992).
86. Martyna, G. J., Tobias, D. J. & Klein, M. L. Constant pressure molecular dynamics algorithms. *J. Chem. Phys.* **101**, 4177–4189 (1994).
87. Tuckerman, M., Berne, B. J. & Martyna, G. J. Reversible multiple time scale molecular dynamics. *J. Chem. Phys.* **97**, 1990–2001 (1992).
88. Darden, T., York, D. & Pedersen, L. Particle mesh Ewald: An N·log(N) method for Ewald sums in large systems. *J. Chem. Phys.* **98**, 10089–10092 (1993).
89. Essmann, U. *et al.* A smooth particle mesh Ewald method. *J. Chem. Phys.* **103**, 8577–8593 (1995).
90. Kräutler, V., van Gunsteren, W. F. & Hünenberger, P. H. A fast SHAKE algorithm to solve distance constraint equations for small molecules in molecular dynamics simulations. *J. Comput. Chem.* **22**, 501–508 (2001).
91. Ramírez-Aportela, E., López-Blanco, J. R. & Chacón, P. FRODOCK 2.0: Fast protein-protein docking server. *Bioinformatics* **32**, 2386–2388 (2016).
92. Garzon, J. I. *et al.* FRODOCK: A new approach for fast rotational protein-protein docking. *Bioinformatics* **25**, 2544–2551 (2009).
93. Gray, J. J. *et al.* Protein-protein docking with simultaneous optimization of rigid-body displacement and side-chain conformations. *J. Mol. Biol.* **331**, 281–299 (2003).
94. RDKit: Open-source cheminformatics.
95. O'Boyle, N. M. *et al.* Open Babel: An open chemical toolbox. *J. Cheminform.* **3**, (2011).

ARTICLE IN PRESS

ARTICLE IN PRESS

96. Trott, O. & Olson, A. J. AutoDock Vina: improving the speed and accuracy of docking with a new scoring function, efficient optimization, and multithreading. *J Comput Chem* **31**, 455–461 (2010).
97. Olechnovič, K. & Venclovas, Č. VoroMQA: Assessment of protein structure quality using interatomic contact areas. *Proteins: Structure, Function and Bioinformatics* **85**, 1131–1145 (2017).
98. Olechnovič, K. & Venclovas, C. D. S. VoroMQA web server for assessing three-dimensional structures of proteins and protein complexes. *Nucleic Acids Res.* **47**, W437–W442 (2019).
99. Rodrigues, J. P. G. L. M. *et al.* Clustering biomolecular complexes by residue contacts similarity. *Proteins: Structure, Function and Bioinformatics* **80**, 1810–1817 (2012).
100. Vangone, A., Spinelli, R., Scarano, V., Cavallo, L. & Oliva, R. COCOMAPS: A web application to analyze and visualize contacts at the interface of biomolecular complexes. *Bioinformatics* **27**, 2915–2916 (2011).
101. Sintchak, M. D. *et al.* Structure and mechanism of inosine monophosphate dehydrogenase in complex with the immunosuppressant mycophenolic acid. *Cell* **85**, 921–930 (1996).

Acknowledgements.

We thank Dr. Daniel Reynes (Emory University School of Medicine) for IMPDH2 cDNA, and Dr. Scott Wilson (U. Alabama) and Dr. Min Jae Lee for *Usp14*$^{-/-}$ MEFs cells, Dr. Marta Taulés (Molecular interaction analysis Technology, CCiTUB) for SPR analysis, Carles Bonet (Genomics and Transcriptomics core service, BMB) for qPCR analysis, Dr. Lluís Ribas (IRB-Barcelona) for lentiviral vectors, and Dr. Cristina Mayor-Ruiz and Dr. Jordi Casanova for their help with reagents. The authors are thankful to Dr. Adolfo Ferrando and Dr. Clara Reglero (Columbia U.) for insightful ideas, and to Dr. Gemma Triola and Dr. Ignacio Alfonso for their critical reading of the manuscript. The authors thankfully acknowledge the use of the computational resources of the *Consorci de Serveis Universitaris de Catalunya* (CSUC) and of the *Centro de Supercomputación de Galicia (CESGA)*. We thank Albaha University for their funding to A.A. This work was supported with grants by Spanish Ministry of Science and Innovation (PID2020-113813RB-I00 and PID2023-146670OB-C21) and the European Commission – NextGenerationEU (Regulation EU 2020/2094), through CSIC's Global Health Platform (PTI Salud Global) and Generalitat de Catalunya (2021-SGR-00504).

Author contributions

MC, TR, AZ, NGS, AGA and BCM performed the biochemical and biological experiments. HC, JLA, and AA synthesized the compounds. PFN generated and provided cell lines. JB performed the computational analysis. JC, AD, JB, GF, and BC designed the research. JB, GF and BC wrote the manuscript with contributions of all authors. Bernat Coll-Martínez, BCM; Bernat Crosas, BC.

Competing interests

Authors declare no competing interests.

ARTICLE IN PRESS

ARTICLE IN PRESS

ARTICLE IN PRESS

ARTICLE IN PRESS

Figure legends

Figure 1. Proteasome structure and conceptual design. (a) View of the proteasome structure (PDB 7W3H[17]) showing the region close to USP14 and highlighting proximal subunits and relevant regions. IU1 binding site is pointed out with a green arrow. The proximity of USP14 to the ATPase motor is highlighted with a yellow arrow. (b) Targeted protein degradation with classical E3 Protacs or with proteasome-directed 26S-UIDs. POI: Protein of Interest; E3: E3-ubiquitin ligase. (c) Structures of the chimeras studied in this work and of the ligands and intermediates from where they were developed.

Figure 2. Structures of USP and IMPDH with bound ligands, and calculated USP14/354/IMPDH2 ternary complex. Structures of (**a**) USP14 with a bound **IU1-248** molecule (PDB 6IIN[17]) and of (**b**) IMPDH2 (PDB 1JR1[101]) with a docked **VX-497** molecule[44] . Ligands are shown with yellow C-atoms and the proteins are represented as blue and red surfaces, respectively. (**c**) Superposition of 10 snapshots from a 500 ns MD simulation of the **HPA-14_PEG3** ligand bound into the CERT1. Red arrows and circles denote the attachment points to build the 26S-UIDs molecules. Chemical structures of compounds are shown in Fig. 1c and Supplementary Fig. 1. (**d**) Ternary complex determined by PROTAC-Model[46] for the protein pair USP14/IMPDH2 with chimera **300** (Fig. 1c). The inset shows the detail of the chimera disposition. (**e**) The same complex superimposed on the structure of 26S (PDB 5GJQ[47]), showing that there is no significant clash between the IMPDH2 protein target and other 26S components. Source data are provided as a Source Data file.

Figure 3. Proteolytic profile of chimeras targeting IMPDH2 and functional impact. (**a**) HeLa cells were treated with 26S-UIDs, **VX-497** or DMSO (vehicle control) for 96 h, then cells were lysed and proteins were analyzed by immunoblotting using anti-IMPDH2 and anti-actin (**300**, **330** and **329**) or anti-GAPDH (**354** and **VX-497**) (Loading). (**b**) Histograms showing the mean ± SD of densitometric analyses of replicates of these assays (n=4 to 11 individual experiments). The asterisk indicates statistical significance over DMSO (one-way ANOVA and Dunnett's multiple comparisons test; P<0.05). (**c**) Left, dose-response effect of **354** on cell viability in HeLa cells and HeLa clone 522-4. Right, dose-response effect of compounds **354**, **VX-497** and **352** on cell viability in HeLa. Cells were treated with different concentrations of compounds or DMSO (control) and cell viability was determined by the MTT assay after 72 h incubation. See curve adjustments in methods section. (**d**) Effect of proteasome inhibitors bortezomib (10 μM) and marizomib (10 nM) on the activity of chimeras **300** (10 μM) in HeLa and **354** (1-10 μM) in HeLa 522-4, which overexpresses IMPDH2-GFP. Cells were treated with **300** and **354** for 96 h. Inhibitors were added 16 h before cell collection. (**e**) Effect of E1 Ub-activating enzyme inhibitor MLN7243 (500 nM) on the activity of chimeras **300** (10 μM) and **354** (1 μM) in HeLa cells. Cells were treated with **300** and **354** for 72 h. The inhibitor was added 8 h before cell collection. (**f**) Effect of **VX-497** (top) and **352** (bottom) on the target degradation by **354**. HeLa cells were treated with **354** (2 μM) and **VX-497** or **352**, at the shown concentrations for 72 h. (**g**) IMPDH2 degradation by **354** in wild-type (WT) and *Usp14*$^{-/-}$ MEFs. Cells were treated during 96 h with 2 μM **354**. Histograms show the mean ± SD of densitometric analyses for replicates of these assays (n = 4 individual experiments). The asterisk indicates statistical significance over DMSO (one-way ANOVA and Tukey's multiple comparisons test; P<0.05). In **c** and **g**, n corresponds to biological replicates. In **a**, **d**, **e**, **f** and **g**, representative immunoblots using IMPDH2 and loading control antibodies are shown. Source data are provided as a Source Data file.

Figure 4. Degradation of CERT1 by 26S-UIDs in MDA-MB-231 cells. (**a**) CERT1 degradation time-course with **368** (10 μM). Treatments showed degradation upon 16 h. (**b**) CERT1 degradation by the indicated chimeras (1-40 μM, 24 h) differing in the linker chain length. Representative immunoblots are depicted. (**c**) Histograms showing the mean ± SD of densitometric analyses of western blots shown in (**b**) (n = 3 to 5 individual experiments). The asterisk indicates statistical significance over DMSO (one-way ANOVA and Dunnett's multiple comparisons test; P<0.05). Source data are provided as a Source Data file.

Figure 5. Mechanism of action of 26S-UIDs in CERT1 degradation. (**a**) Effect of the proteasome inhibitor marizomib (Mar) (0.5 μM, 3 h preincubation), the E1-Ub activating enzyme inhibitor MLN7243 (0.2 μM, 3 h preincubation) and the CERT1 truncated 26S-UIDs **366** (100 μM, 3 h preincubation) on **368**-induced CERT1 degradation (10 μM, 24 h incubation). Accumulation of K48-linked ubiquitylated proteins confirms proteasome inhibition by marizomib, while the absence of ubiquitinated histone H2A/H2B proves the effectiveness of MLN7243 (Veh., DMSO control). (**b, c**) CERT1 degradation by **386** in the presence of different concentrations of truncated 26S-UIDs **366** and **352** (shown in Fig. 1c) in 24 h culture after 3 h preincubation with the competitor. (**d, e**) Contribution of autophagy to **386**–induced CERT1 degradation. In (**d**), 3 h before 26S-UIDs addition, cells were treated or not with marizomib as in **a** in the presence or absence of protease inhibitors (PI: E64D, 10 μg/mL;

ARTICLE IN PRESS

pepstatin A, 5 µg/mL). Medium was renewed and cells were treated for 24 h with **386** (10 µM) in the absence or presence of PI. In (**e**), cells were treated for 3 h with marizomib or vehicle as in **a**. Medium was renewed, cells were treated for 20 h with **386** (10 µM) and then chloroquine (Chl) or vehicle were added and cells were collected 4 h after Chl addition. (**f**) CERT1 degradation by **368** at two concentrations and 16 h treatments in WT and *Usp14*$^{-/-}$MEFs. In **a** and **f**, asterisks indicate statistical significance (one-way ANOVA and Tukey's multiple comparisons test; P<0.05). Representative immunoblots are shown. In **a** and **f**, n corresponds to biological replicates. Source data are provided as a Source Data file.

Figure 6. Effect of the indicated degraders on the levels of ceramides. Compounds were used at 10 µM (**a** and **b**) or 20 µM (**c**) and incubation times were 24 h, except for MDA-MB-231 cells (48 h). Data are the mean ± SEM of 3 to 4 experiments with triplicates. Asterisks indicate statistical significance at P ≤ 0.05 (one-way ANOVA and Tukey's multiple comparisons test). In *y* axis, n corresponds to biological replicates. Source data are provided as a Source Data file.

Figure 7. Representative ternary complexes of (a) USP14/354/IMPDH2 and (b) USP14/368/CERT1. USP14 is represented as blue ribbons and sticks, IMPDH2 and CERT1 as red ribbons and sticks, the 26S-UIDs as yellow sticks, and hydrogen bonds and pi-pi interactions as yellow and green dashed lines, respectively. (**c**, **d**) The same complexes with USP14 represented as a gray surface. The cyan-colored patches correspond to the USP14 interacting surface. Source data are provided as a Source Data file.

ARTICLE IN PRESS

Editor's Summary

Targeted Protein Degradation (TPD) relies on the binding of specific targets and E3 ubiquitin-ligases to promote ubiquitination and degradation of targets by the proteasome. Here, by designing chimeras that bind the proteasome-associated factor Usp14, the authors present a generalizable TPD approach based on proteasome-dependent and E3 ligase-independent small-molecule compounds.

Peer Review Information: *Nature Communications* thanks the anonymous reviewer(s) for their contribution to the peer review of this work. A peer review file is available.

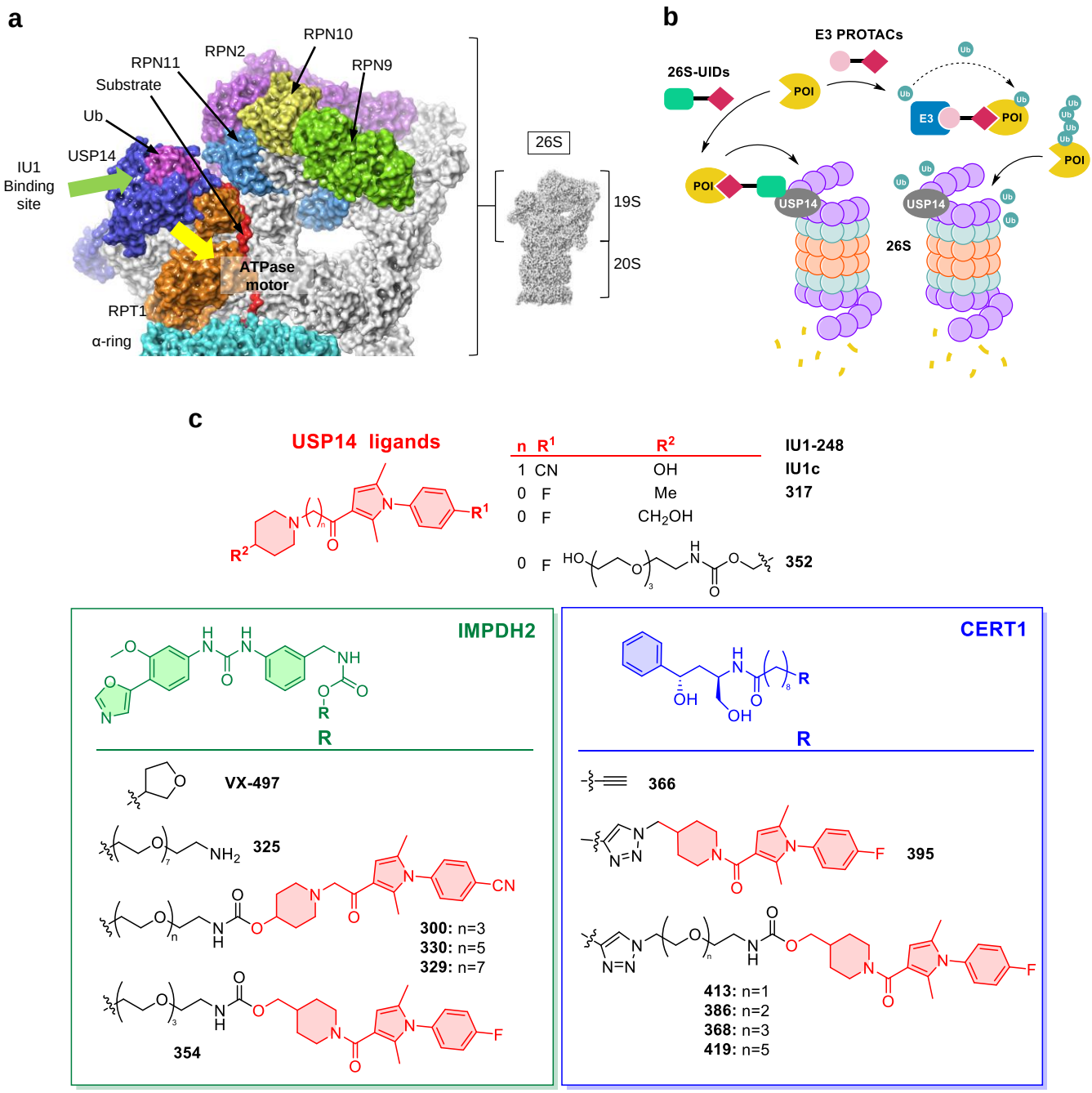
a
RPN10
RPN2
RPN11
RPN9
Substrate
Ub
USP14
IU1
Binding
site
ATPase
motor
RPT1
α-ring
26S
19S
20S
b
E3 PROTACs
26S-UIDs
POI
E3
Ub
USP14
26S
c
USP14 ligands
n R1 R2
1 CN OH IU1-248
0 F Me IU1c
0 F CH2OH 317
0 F 352
IMPDH2
R
VX-497
325
300: n=3
330: n=5
329: n=7
354
CERT1
R
366
395
413: n=1
386: n=2
368: n=3
419: n=5

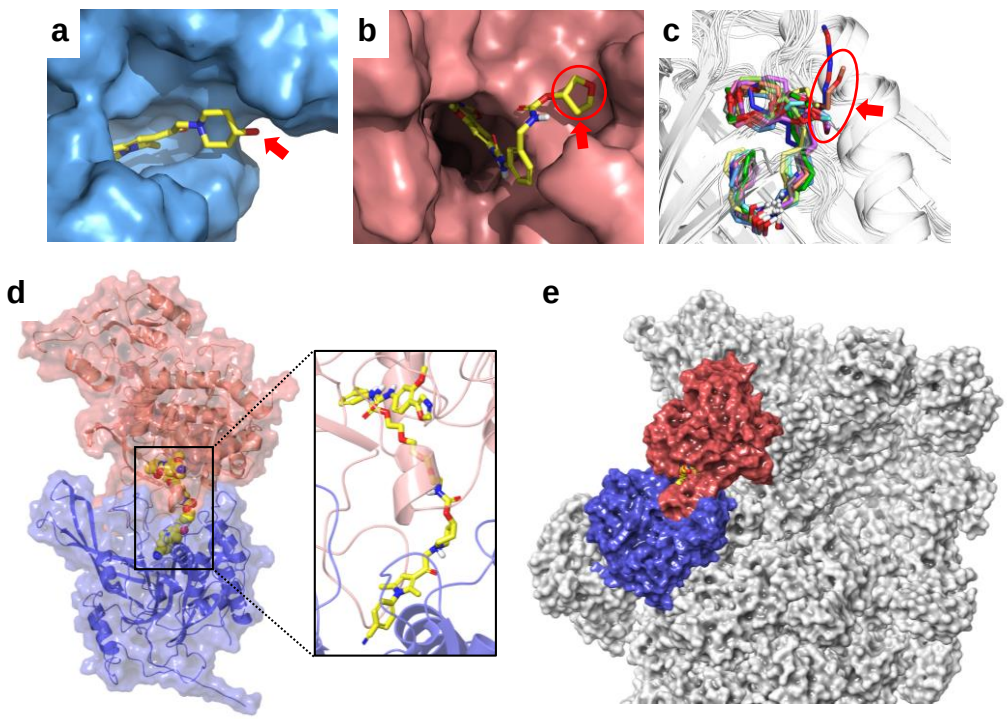
a
b
c
d
e

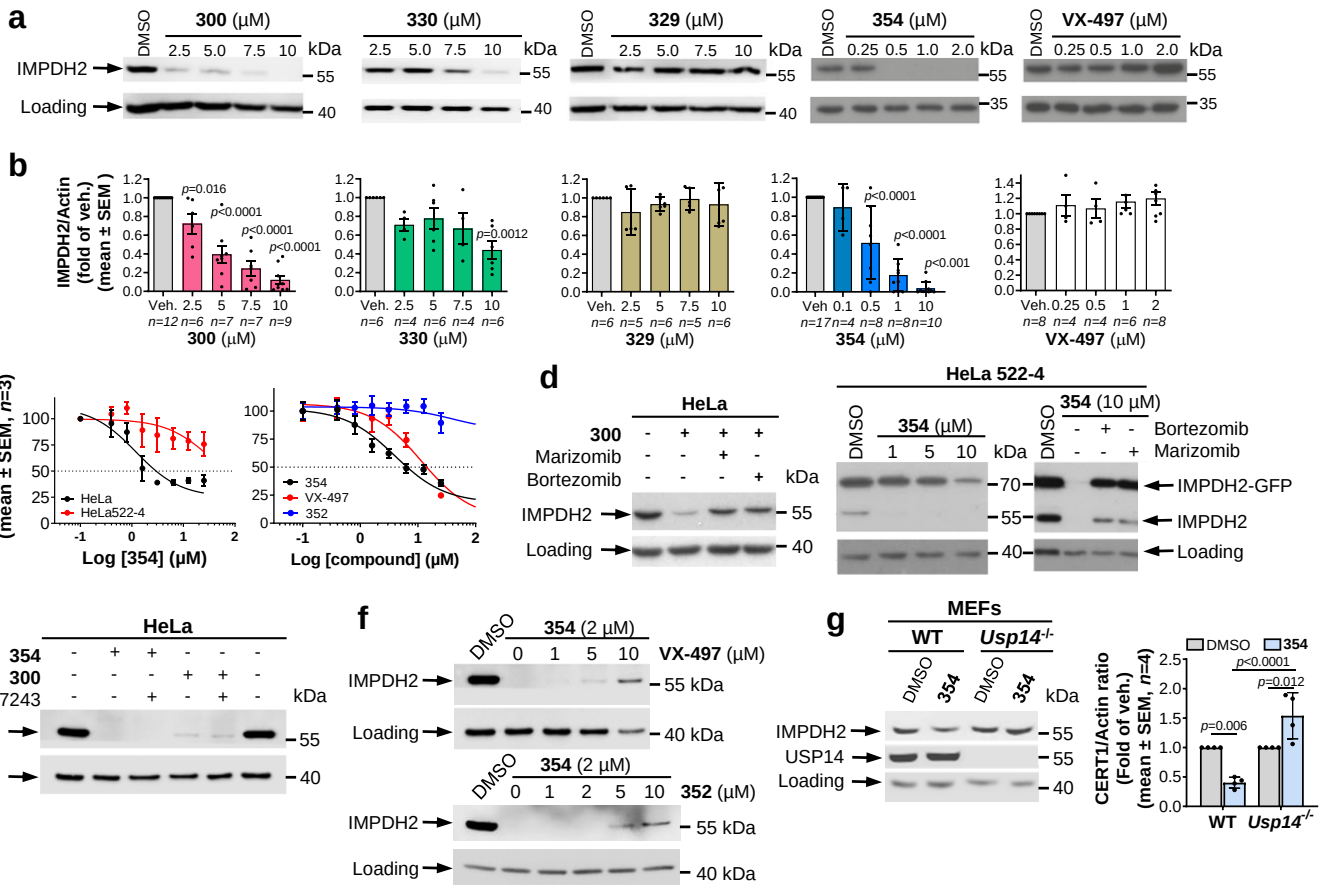
a
DMSO
300 (μM)
2.5 5.0 7.5 10 kDa
330 (μM)
329 (μM)
354 (μM)
0.25 0.5 1.0 2.0
VX-497 (μM)
IMPDH2
Loading
55
40
35
b
IMPDH2/Actin (fold of veh.) (mean ± SEM)
p=0.016
p<0.0001
p=0.0012
p<0.001
Veh. 2.5 5 7.5 10
Veh 0.1 0.5 1 10
Veh. 0.25 0.5 1 2
n=12 n=6 n=7 n=7 n=9
n=6 n=4 n=6 n=4 n=6
n=6 n=5 n=6 n=5 n=6
n=17 n=4 n=8 n=8 n=10
n=8 n=4 n=4 n=6 n=8
c
Cell viability (% of vehicle) (mean ± SEM, n=3)
HeLa
HeLa522-4
Log [354] (μM)
354
VX-497
352
Log [compound] (μM)
d
HeLa
300
Marizomib
Bortezomib
HeLa 522-4
354 (μM)
354 (10 μM)
Bortezomib
Marizomib
IMPDH2-GFP
IMPDH2
e
HeLa
354
300
MLN7243
f
354 (2 μM)
VX-497 (μM)
352 (μM)
55 kDa
40 kDa
g
MEFs
WT
Usp14-/-
USP14
CERT1/Actin ratio (Fold of veh.) (mean ± SEM, n=4)
p=0.006
p<0.0001
p=0.012

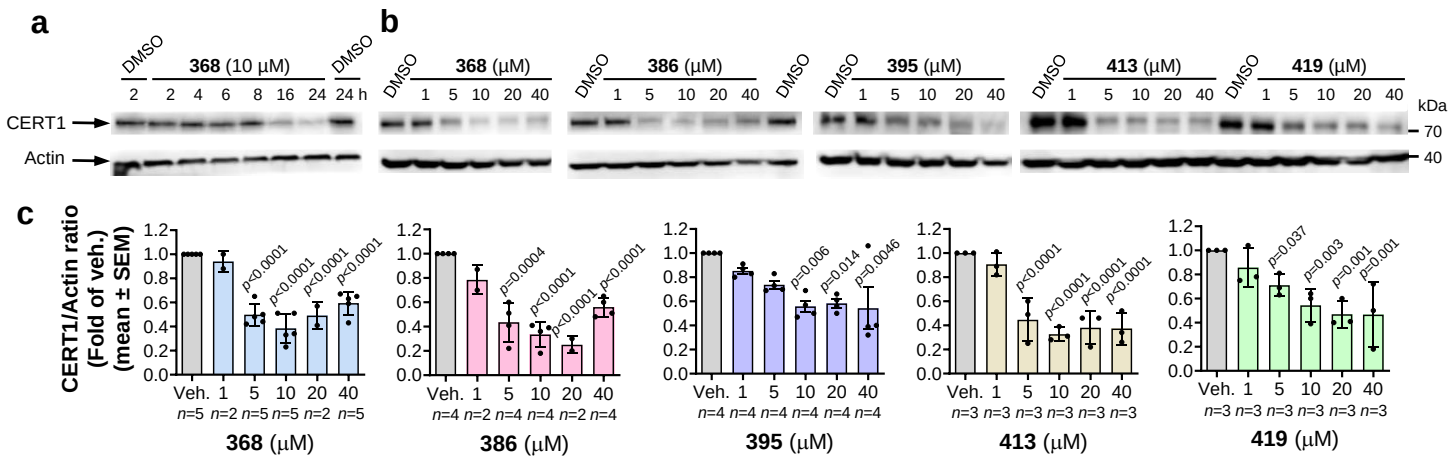
a
b
DMSO
368 (10 μM)
DMSO
2 2 4 6 8 16 24 24 h
DMSO
368 (μM)
1 5 10 20 40
DMSO
386 (μM)
1 5 10 20 40
DMSO
395 (μM)
1 5 10 20 40
DMSO
413 (μM)
1 5 10 20 40
DMSO
419 (μM)
1 5 10 20 40
kDa
CERT1
Actin
70
40
c
CERT1/Actin ratio
(Fold of veh.)
(mean ± SEM)
p<0.0001 p<0.0001 p<0.0001 p<0.0001
Veh. 1 5 10 20 40
n=5 n=2 n=5 n=5 n=2 n=5
368 (μM)
p=0.0004 p<0.0001 p<0.0001 p<0.0001
Veh. 1 5 10 20 40
n=4 n=2 n=4 n=4 n=2 n=4
386 (μM)
p=0.006 p=0.014 p=0.0046
Veh. 1 5 10 20 40
n=4 n=4 n=4 n=4 n=4 n=4
395 (μM)
p<0.0001 p<0.0001 p<0.0001 p<0.0001
Veh. 1 5 10 20 40
n=3 n=3 n=3 n=3 n=3 n=3
413 (μM)
p=0.037 p=0.003 p=0.001 p=0.001
Veh. 1 5 10 20 40
n=3 n=3 n=3 n=3 n=3 n=3
419 (μM)

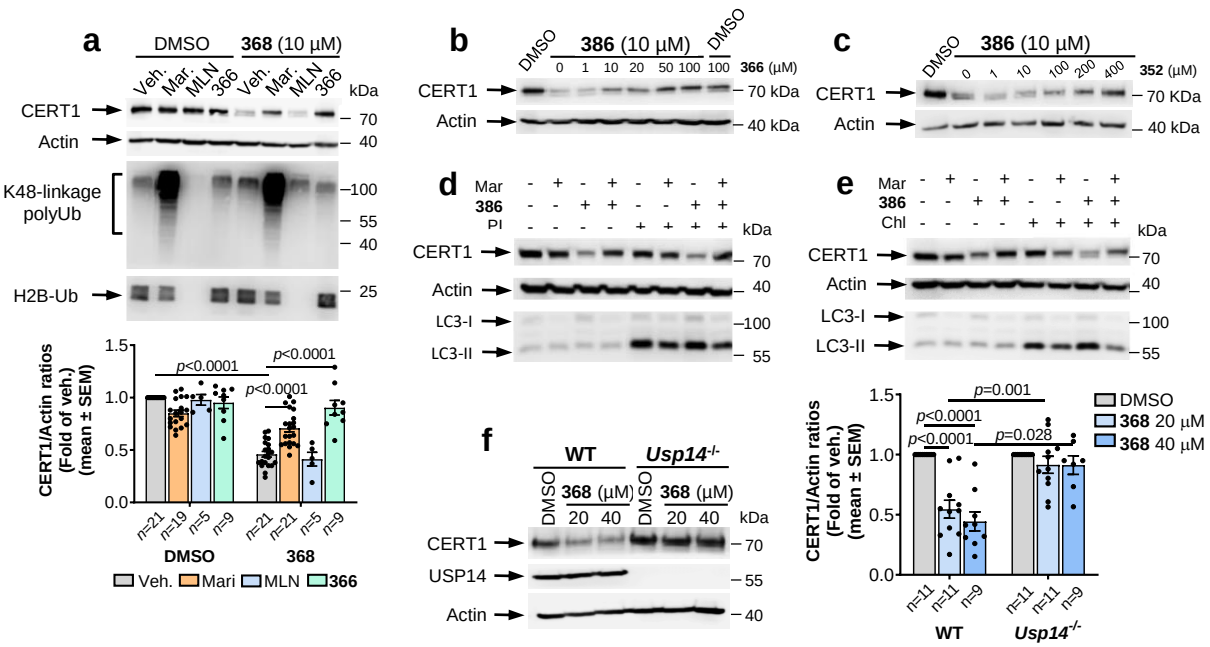
a
DMSO
368 (10 μM)
Veh.
Mar.
MLN
366
kDa
CERT1
Actin
K48-linkage polyUb
H2B-Ub
70
40
100
55
25
CERT1/Actin ratios (Fold of veh.) (mean ± SEM)
p<0.0001
n=21
n=19
n=5
n=9
DMSO
368
Veh.
Mari
MLN
366
b
386 (10 μM)
0 1 10 20 50 100 100 366 (μM)
70 KDa
40 kDa
c
352 (μM)
0 1 10 100 200 400
d
Mar
386
PI
LC3-I
LC3-II
e
Chl
f
WT
Usp14-/-
368 (μM)
20 40
USP14
p=0.001
p=0.028
n=11
DMSO
368 20 μM
368 40 μM

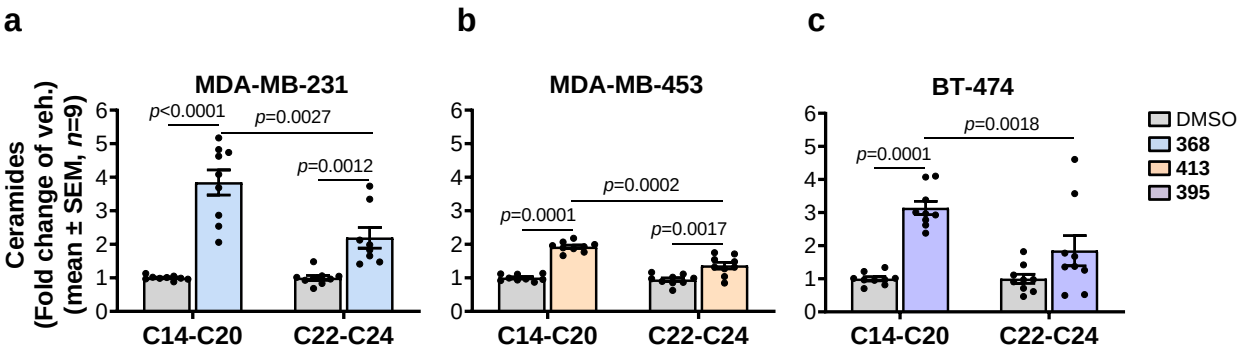
a
b
c
MDA-MB-231
MDA-MB-453
BT-474
Ceramides
(Fold change of veh.)
(mean ± SEM, n=9)
p<0.0001
p=0.0027
p=0.0012
p=0.0001
p=0.0002
p=0.0017
p=0.0001
p=0.0018
C14-C20
C22-C24
DMSO
368
413
395

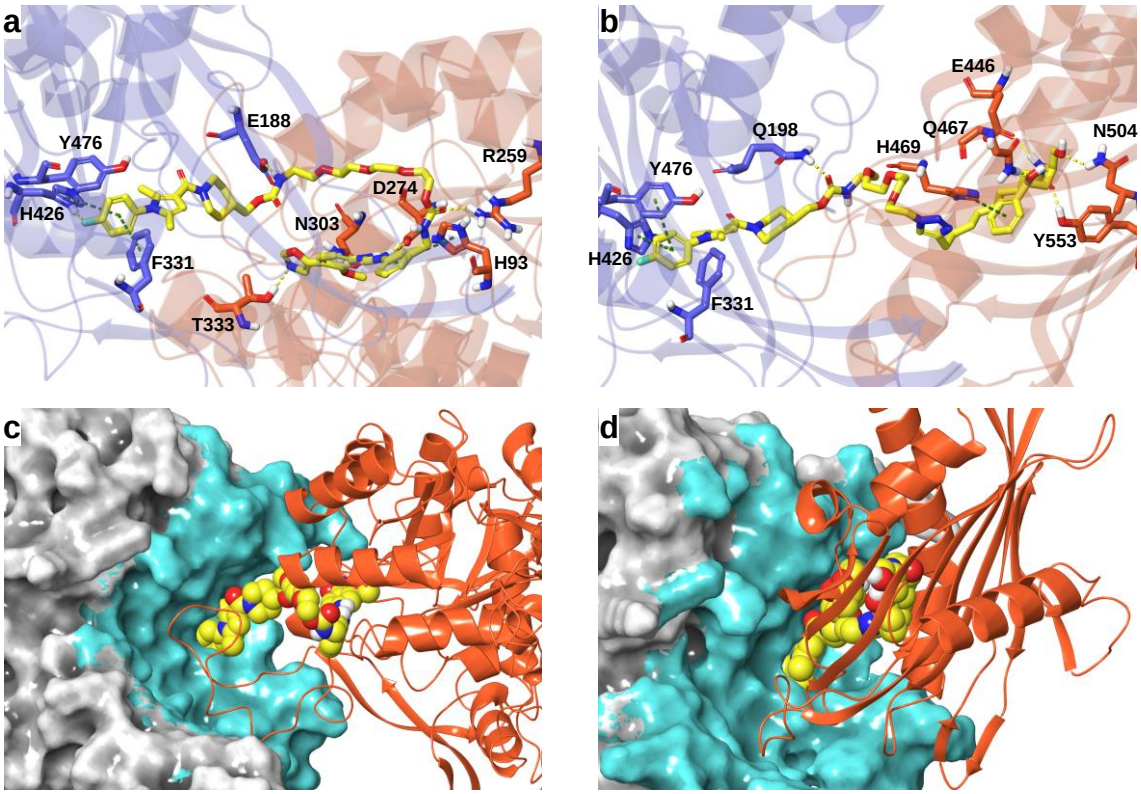
a
Y476
E188
R259
D274
H426
N303
F331
H93
T333
b
E446
Q198
Q467
N504
H469
Y476
Y553
H426
F331
c
d